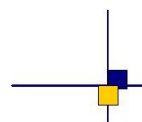


GUT2 WP6000 Final Report



Reference: CLS-DOS-NT-11-128

Nomenclature: EUROPE

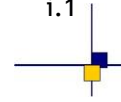
Issue: 2 rev 0

Of the: 30 September 2011



CLS 8-10 Rue Hermès - Parc Technologique du Canal - 31520 Ramonville St-Agne - FRANCE

Téléphone 05 61 39 47 00 Télécopie 05 61 75 10 14



Chronology Issues:

Issue:	Date:	Reason for change:
V2	30/09/2011	New input from DTU and UH

People involved in this issue:

Written by (*):		Date + Initials:(visa ou ref)
	MH Rio	
	G.Dibarboure	
	P. Knudsen	
	O. Andersen	
	F. Siegesmund	

Distribution:

Company	Means of distribution	Names
ESA	Electronic file	J. Benveniste S. Dinardo B. Lucas
CLS	Notification	

List of tables and figures

List of tables:

Table 1. Summary on the use of different corrections on mean profiles. (See Rio and Andersen, 2009 for details and figures) including a 7 years mean profiles (1993-1999) for TP (cycles from 12 to 268) and a 6 years mean profiles (1996-2001) for ERS-2	2
Table 2: Overview of Sea Level Anomaly Errors associated with the temporal reference. Error terms A to D are present on all <SSH> temporal references (repeat track analysis or gridded MSS), and terms E to I are specific to gridded mean sea surfaces (geodetic altimetry or uncharted repetitive track).	4
Table 3: The set of range and geophysical corrections applied for CLS01, CLS10, DNSC08 and DTU10MSS. Only corrections applied to the TOPEX/Poseidon and Jason-1 have been shown. The corrections applied to different satellites missions (ERS1, ERS2, GEOSAT, GFO etc) included in the determination of the MSS will be different	22
Table 4: The state of the art range and geophysical corrections.	23
Table 5: Mean and standard deviation between recent MSS models. The values above the diagonal is the mean difference in cm. The values below the diagonal are the standard deviation between the models in cm. The numbers in brackets are the standard deviation once outliers > 1 meter has been removed	27

List of figures:

Figure 1: Formal mapping error (cm) of the CLS/CNES MSS gridding process (OI)	1
Figure 2 : Unit cm. Difference between a simple T/P average (cycles 11-268) and T/P+Jason1 average (cycles 11-353 & 11-250). Processing and standards are identical, inter-annual variability has been minimized with multi-mission maps. Regional RMS = 0.85cm.	6
Figure 3 : Differences (m) between DTU10 and CLS/ CNES10 before (top) and after (middle) inter-annual oceanic variability is minimized with the difference between a 17 year average and a 93-99 average from DUACS multi-mission maps (bottom map).	7
Figure 4 : Error H+I. Standard deviation of the along-track sea surface anomaly (cm) from T/P and Jason (pass-band filtered from 100km to 500km), before, during and after the orbit change.	12
Figure 5 : Error G. Along-track difference (m) between the MPs and two gridded MSS computed with (plain) or without (dotted) the GFO dataset. Differences are limited to WL<100km by the gridding process (solution constrained by other repetitive datasets). The along-track profile is computed on GFO track #147.	13
Figure 6 : Error E. Residuals (cm) between the CNES/CLS 2010 MSS and the ERS/ENVISAT mean track (data actually used in the MSS gridding).	14
Figure 7 : Error E+F+I. Differences (m) between CNES/CLS2010 (left) or DTU10 (right) and EGM08.	17
Figure 8 : Error F+H2+I2. Differences (m) between DNSC/DTU10 (top) or CNES/CLS 2010 (bottom) & EGM08 after high-pass filtering (75km).	18
Figure 9 : Error I+H. Raw differences (m) between CLS01 and EGM08 (left), CLS/CNES 10 and CLS01 (middle), and CNES/CLS10 and EGM08 (right). Red diamonds located between ERS/ENVISAT tracks (green circles) highlight the improved minimization of mesoscale handling in geodetic data	19

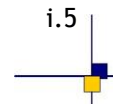
Figure 10 : Artefact created by the mesoscale minimization process from the MSS gridding process. Some rare isotropic seamounts that were correctly resolved by the CLS01 MSS or the DTU10 (right) were smoothed in the CLS/CNES10 (middle). A change in the CLS/CNES10 gridding process can restore the original information from geodetic data (left).	20
Figure 11: The root square sum of the difference between the 6 corrections shown in Table 4 and representing the largest effect of using different state of the art corrections to MSS determination.	24
Figure 12: RMS of the difference between state of the art range and geophysical correction interpolated from six years Jason-1 profile (left) and six years Envisat profiles (right).	26
Figure 13: Spatial error variance computed from the difference between the two most recent independent MSS models. The CLS01MSS and the DNSC08 MSS. The upper figure shows the error variance associated with the difference (in cm^2). The lower figure shows the correlation length of the "error" The difference between the CLS01 and DNSC08 MSS used for this computation is shown in Figure 15	28
Figure 14: Spatial error variance for the range and geophysical errors in $\text{cm}^2 \times 100$.	29
Figure 15: Correlation length in km of the range and geophysical error estimate.	30
Figure 16: Location of the four typical regions selected to illustrate the different behavior of the error covariances associated with the use of different range and geophysical corrections. The underlying figure is the difference between the two most recent independent MSS models (the CLS01 MSS and the DTU08MSS model) given in cm.	31
Figure 17. The covariance functions for the errors in the range and geophysical corrections for 6 year mean Jason profiles.	31
Figure 18: Two dimensional covariance function for the centre of the North Atlantic region for each of the range and geophysical errors for 6 year mean Jason profiles	32
Figure 19: Two dimensional covariance function for the centre of the North Atlantic region for each of the range and geophysical errors for 6 year mean Envisat profiles	33
Figure 20: The covariance functions for the errors in the range and geophysical corrections for 6 year mean Jason profiles.	34
Figure 21: Two dimensional covariance function for the center of the North Atlantic region for each of the range and geophysical errors for 6 year mean Jason-1 profiles	35
Figure 22: The covariance functions for the errors in the range and geophysical corrections sampled in 6 year mean Jason profiles.	36
Figure 23: Two dimensional covariance function for the center of the North Atlantic region for each of the range and geophysical errors for 6 year mean Jason-1 profiles	37
Figure 24: The covariance functions for the errors in the range and geophysical corrections for 6 year mean Jason profiles. Notice that the scale on the vertical axis should be $10 \times \text{cm}^2$ like for the previous figures	38
Figure 25:Two dimensional covariance function for the Antarctica region for each of the range and geophysical errors for 6 year mean Jason-1profiles	39
Figure 26: MDT error components given as square root of degree variances, for a given degree (top) and accumulated (bottom).	41
Figure 27: Difference in assimilated MDT [m], depending on the applied MSS (CLS10- DTU10).	43
Figure 28: Difference in modeled MDT [m] (GECCO-CLS - GECCO-DTU)..	44
Figure 29: MDT residuals [m] for converged GECCO solutions for (top) GECCO-DTU and (bottom) GECCO-CLS.	45

Figure 30: MDT residuals [m] from GECCO-CLS optimization compared to a priori MDT error, given as square root of degree variances for specific degree (top) and accumulated (bottom).

46

Figure 31: Same as Fig. 30, but with increased MSS mapping error.

47

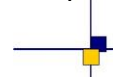


Applicable documents / reference documents

- Andersen, O. B., and R. Scharroo (2010), Range and geophysical corrections in coastal regions, book chapter in eds. (Vignudelli i et al), Coastal altimetry, ISBN: 978-3-642-12795-3
- Andersen O. B, Knudsen P (2009) The DNSC08 mean sea surface and mean dynamic topography. *J. Geophys. Res.*, 114, C11, doi:10.1029/2008JC005179, 2009
- Andersen, O. B., P. Knudsen and P. Berry (2010) [The DNSC08GRA global marine gravity field from double retracked satellite altimetry](#), *Journal of Geodesy*, Volume 84, Number 3, DOI: [10.1007/s00190-009-0355-9](#)
- Fu, L., and A. Cazenave (2001), *Satellite Altimetry and Earth Sciences. A Handbook of Techniques and Applications*, Academic Press, 460 pp.
- Hernandez, F., and P. Schaeffer (2000), Altimetric Mean Sea Surfaces and Gravity Anomaly maps inter-comparisons *AVI-NT-011-5242-CLS*, 48 pp. CLS Ramonville St Agne, France
- Köhl, A., and D. Stammer, 2008, Variability of the meridional overturning in the North Atlantic from the 50 years GECCO state estimation, *J. Phys. Oceanogr.*, 38, 1913-1930.
- Knudsen, P. (1993), Satellite altimetry for geodesy and geophysics, in (ed) J. Kakkuri, *lecture notes for NKG autumn school*, Korpilampi, Finland, p. 87-126.
- Maltrud, M.E. and J.L. McClean, 2005, An eddy resolving global 1/10 degree ocean simulation. *Ocean Modelling*, 8, 31-54.
- Marshall, J., A. Adcroft, C. Hill, L. Perelman, and C. Heisey, 1997, A finite-volume, incompressible Navier Stokes model for studies of the ocean on parallel computers, *J. Geophysical Res.*, 102 (C3), 5753-5766.
- Parke, M. E., R. H. Steward, D. L. Farless and D. E. Cartwright, On the choice of orbits for an altimetric satellite to study ocean circulation and tides. *J. Geophys Res.*, 92, 11693-11707, 1987.
- Rio M.-H. And O. Andersen, GUT WP8100 Standards and recommended models, WP8100, ESA-ESRIN, Frascati, Italy, GUT Toolbox, Internal Report, 2009.
- Siegismund, F.; A. Köhl; and D. Stammer, 2010, Inferring the mean dynamic topography by using GOCE geoid information in ocean state estimations, in Münch, U; and W. Dransch (eds.) *Observation of the System Earth from Space*, Geotechnologien Science Report 17, 101-105, Koordinierungsbüro Geotechnologien, Potsdam, ISSN 1619-7399
- Wunsch, C., 1996, *The ocean Circulation Inverse Problem*, Cambridge University Press, 458 pp.

Contents

1. INTRODUCTION.....	1
2. Identifying the main MSS error sources	4
2.1. Overview of the MSS error sources	4
2.2. Errors #A and #B: mesoscale and inter-annual variability.....	5
2.3. Error terms #C : geophysical corrections	8
2.4. Error term #D: cross-track geoid gradient.....	8
2.5. Errors E to I	9
2.5.1. Internal comparisons based on CLS/CNES data.....	11
2.5.2. Differences between recent MSS.....	15
3. ESTIMATING THE CONTRIBUTION OF GEOPHYSICAL CORRECTIONS UNCERTAINTIES IN THE MSS VARIANCE AND COVARIANCE ERROR BUDGET.	22
3.1. Impact of range and geophysical correction errors.	22
3.2. Covariance functions for typical regions.	30
3.2.1. North Atlantic Region	31
3.2.2. Tropical Pacific Region	34
3.2.3. South East Asian region	35
3.2.4. Antarctic Region	38
4. MSS Error Approximation from Ocean State Estimation	40
4.1. Ocean Model and Data Assimilation Methodology	40
4.2. Ocean State Estimation Experiments	42
4.3. MSS error approximation.....	43
Annexe A - List of acronyms	48



1. INTRODUCTION

The objective of this workpackage is to better assess the accuracy of the altimetric Mean Sea Surfaces that are commonly combined to models of the marine geoid to estimate the ocean Mean Dynamic Topography, and, by geostrophy, the ocean mean currents.

The rationale behind this work is to go beyond the theoretical knowledge of the MSS error given as outputs of the MSS gridding process (Figure 1), which is consistent with the RMS cross-over differences of the various mean profiles used in the MSS computation. The MSS error on Figure 1 therefore does not take into account external error sources as the error on the different corrections used to process the altimetric Sea Surface Heights before computing mean profiles.

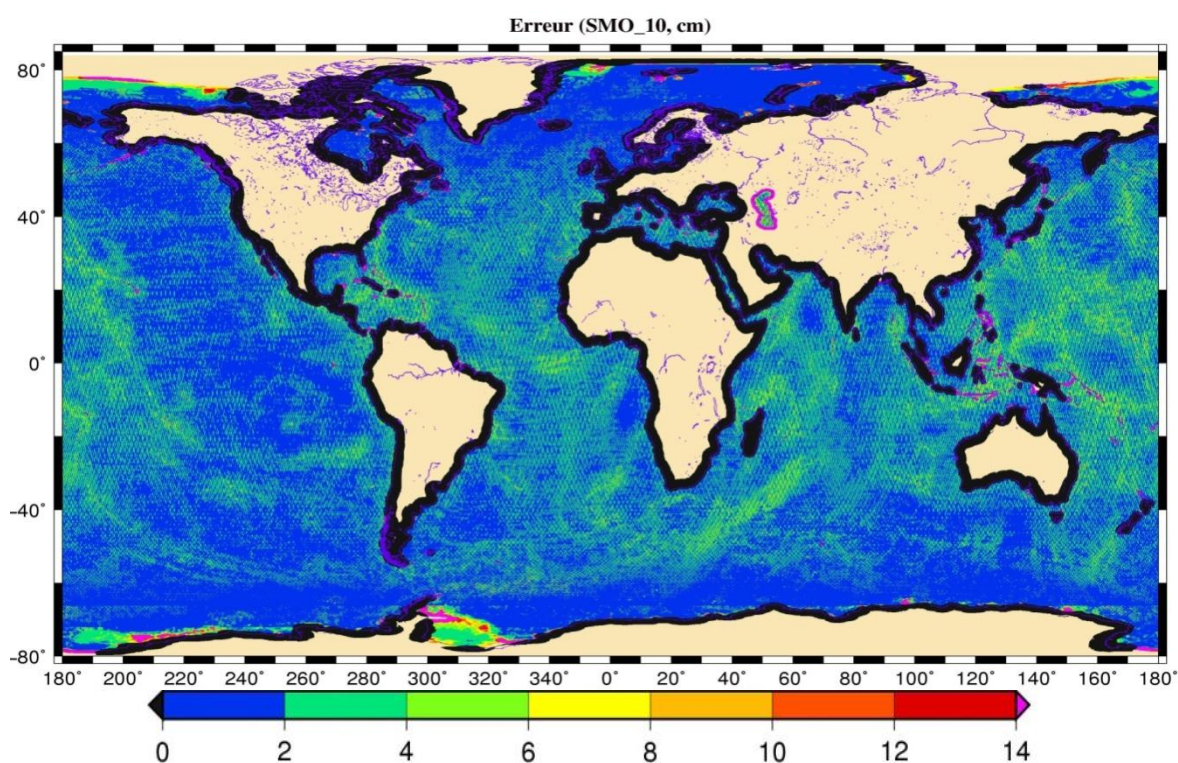


Figure 1: Formal mapping error (cm) of the CLS/CNES MSS gridding process (OI)

This work is a continuation of the work in GUT and the report for WP8000 by Rio and Andersen. The result of the impact of using different corrections for different missions is was described in the GUT WP8000 report and is summarized in Table 1 below.

Mis-sion	Test	Impact on mean	Impact on mean accuracy
Orbit			
J1	GDRC VS GDRB	+/-1 cm Geographical bias btw Pacific + North Atl / Indian + South Atl	Weak local improvements and degradations
EN	ESDC VS CNES	+/-2 cm depending on basins. Global 0.1 cm bias	Global improvement (+6 cm ²) with CNES orbit
TP	GSFC00 VS CNES	+/-3 cm depending on basins. Global 0.7 cm bias	Weak local improvements and degradations
	GSFC05 VS GFSC00	+/-0.3 cm depending on hemisphere - No bias	Weak local improvements and degradations
Iono			
J1	GIM VS ALTIMETER	+/-1 cm depending on latitude. Global 0.1 cm bias	Weak global improvement with ALTIMETER
EN	GIM VS ALTIMETER	0 to +2 cm depending on latitude. Global 0.8 cm bias	Weak global improvement with ALTIMETER
ERS2	GIM VS IRI	-1.7 to 0.3 cm depending on latitude.	
TP	ALTIMETER VS IRI	-1.5 to 0.1 cm depending on latitude	
WET TROPO			
J1	ECMWF VS RADIOMETER	Open ocean: +/- 0.5 cm depending on latitude. in Coastal areas up to 2 cm. No bias	Global improvement (from 5 to 20% of variance) with Radiometer
EN	ECMWF VS RADIOMETER	Open ocean: +/- 0.5 cm depending on latitude. in Coastal areas up to 2 cm. Global 0.6 cm bias	Global improvement (from 5 to 20% of variance) with Radiometer
	NCEP VS ECMWF	+/- 3 cm btw wet and dry areas. Global -0.8 cm bias	Significant improvement with ECMWF (+5 cm ²) mostly in wet areas (>20cm ²)
ERS2	RADIOMETER VS ECMWF	-1.4 to 1.8 cm depending on latitude	
TP	RADIOMETER VS ECMWF	-1.2 to 1.6 cm depending on latitude	
DRY TROPO			
ERS2	ECMWF VS NCEP	+/- 0.2 cm depending on latitude and oceans	
TP	ECMWF VS NCEP	+/- 0.2 cm depending on latitude and oceans	
DAC			
TP	IB VS DAC-HR	+/- 1 cm locally. No global bias	Global improvement: (+ 9 cm ²) with DAC-HR. Stronger in coastal and strong wind variability areas
ERS2	IB Brief vs MOG2D_IB	1.2 to 2.8 cm Global bias due to the static response not included in MOG2D An interesting global pattern of highs and lows, which corresponds to the S2 constituent in the Atmosphere which is included in the MOG2D but not in the inverse barometer	
TP	IB Brief vs MOG2D_IB	2 to 2.8 cms locally Global bias due to the static response not included in MOG2D	
TIDES			
J1	FES04 VS GOT00.2	> 2 cm locally in coastal areas. No bias	Weak global improvement with GOT near the coasts
EN	FES04 VS GOT00.2	> 2 cm locally in coastal areas. No bias	Weak global improvement with GOT near the coasts Improvements with FES at high latitudes
TP	FES04 VS GOT00.2	> 2 cm locally in coastal areas. No bias	Weak global improvement with GOT near the coasts
ERS2	GOT00.2 VS GOT99	> 0.5 cm locally in coastal areas. No bias	Slight global improvement with GOT00 near the coasts
TP	FES04-GOT4.7	+/- 2 cm	
TP	FES04-GOT4.7	+/- 0.2 cm	
SSB			
EN	BM4 VS NPARAM	+/- 3 cm Global 2.6 cm bias	Inhomogeneous impact
TP	BM4 VS NPARAM	+/- 0.5 cm Global 2.4 cm bias	Weak improvement with NPARAM
TP	BM4 VS NPARAM	1.6 to 2.4 cm Global 2 cm bias	

Table 1. Summary on the use of different corrections on mean profiles. (See Rio and Andersen, 2009 for details and figures) including a 7 years mean profiles (1993-1999) for TP (cycles from 12 to 268) and a 6 years mean profiles (1996-2001) for ERS-2

As a follow-on to the GUT WP8000 activity, the objective of this workpackage was to better assess the characteristics of the MSS errors. It is divided into three main parts. The objective of section 2 is to identify and give order of magnitude of the main MSS error sources. In section 3, a specific work has been carried out to quantify the error variance contribution due to the choice of geophysical corrections applied on altimetric heights, as well as to estimate for four specific locations the error covariance function of the MSS error due to this geophysical correction choice. In section 4, the MSS error characteristics are induced from the analysis of ocean models outputs.



2. Identifying the main MSS error sources

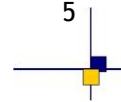
2.1. Overview of the MSS error sources

Gridded MSS estimates are derived from along-track mean profiles or from the original datasets used to build the MPs. Thus any error on the repeat track analysis is also contained in the gridded MSS proxy. Conversely, the gridding process and the use of geodetic data in the MSS creation can add new terms of error. Table 2 gives an overview of the static <SSH> error. Error terms A to D are potentially corrupting along-track mean profiles, while error terms E to I are potentially corrupting gridded MSS.

			Error if not corrected	Current status in DUACS Profiles
Mean Profile Error	A	Uncorrected mesoscale variability error	6mo-1year : 5 to 7cm min (WL: 20-50km) 3-5years: <3.5cm 7-15years: <1cm (WL: 100-200km)	Non-existent. Instantaneous ocean variability is removed before the time average, average computed over 10+ years on all tracks).
	B	Interannual variability error	<5cm (WL: >5000km) <5-8cm in wb currents (WL: 200-500km)	Non-existent as re-referenced on a common period and cross-calibrated on the reference mission (both SSH and <SSH>)
	C	Geophysical corrections errors	>3.8cm (2001, all WL) 3.5cm (2001 standards, WL>50km) >1 to 3cm (GDR-B)	GDR-C or equivalent used for all missions. Remaining error not well-defined.
	D	Cross-track geoid gradient	>2.5 cm if cross-track geoid gradient correction is not used	CTGG applied <1cm between CTGG methods

		MSS computed before 2008	Recent MSS (CLS/CNES, DNSC, DTU)
MSS Error	E	Correlated error averaging (discrepancy between missions → mix of errors)	Difference between cross-calibrated MPs and MSS actually using them : 1 cm (WL < 100km) 1-3 cm (WL > 100km)
	F	Map smoothing (scales which cannot be resolved away from known tracks, degrading along-track content)	Local difference between EGM08 and recent MSS, high-pass filter, located on bathymetry gradients 3 to 5 cm (WL : 10 to 30km + noise) 2 to 5 cm (WL : mesoscale)
	G	Omission error	Small scales(difference between MSS computed with and w/o specific TP or GFO tracks): 1.6 to 2.5cm (WL: <100km)
	H		Larger scales (SSHA increase during on new track if tandem data are not used, difference between CLS01 and CLS10 in ERS diamonds) 3 to 7 cm (WL: all) 1.5 cm (WL: 50 to 500km)
	I	Mesoscale variability from geodetic data not properly removed before absorption in MSS	Best case (SSHA increase during T/P drift using DNSC or CLS/CNES) 1 cm (WL: 100 to 500km) Worst case (different behaviour of CLS and DNSC when compared to a common EGM08): <3 to 5 cm (WL < 75km)

Table 2: Overview of Sea Level Anomaly Errors associated with the temporal reference. Error terms A to D are present on all <SSH> temporal references (repeat track analysis or gridded MSS), and terms E to I are specific to gridded mean sea surfaces (geodetic altimetry or uncharted repetitive track).



The MSS induced error is particularly problematic for three reasons: it is static, it is spatially correlated, and it is the same for all missions using the same <SSH> reference. To that extent, it is barely possible to empirically minimize it with multi-mission cross-calibration methods (e.g. Dibarboure et al, 2010) or with ocean model assimilation.

Sections 2.2 to 2.4 shows how modern repeat track analysis is able to control the error, and section 2.5 focuses on errors induced by the gridding process.

2.2. Errors #A and #B: mesoscale and inter-annual variability

The simplest Mean Profiles are time averages of similarly co-located SSH data from the same ground track. But there are downsides to this simple approach: absorption of mesoscale variability error in the average (error #A from Table 2), and mission-specific discrepancies due to inter-annual variability (error #B).

For such simple averages, mesoscale variability is as large as 5 to 7cm for six-month to one-year averages, and it is averaged out as more data are incorporated into the <SSH>. For repetitive orbits with a 10-day cycle, the error becomes stable once 7 to 10 years have been used and the residual error is inferior to 0.9cm rms in zones of intense mesoscale activity and negligible elsewhere. Figure 2 shows the difference between a simple temporal average from T/P alone and from T/P+Jason.

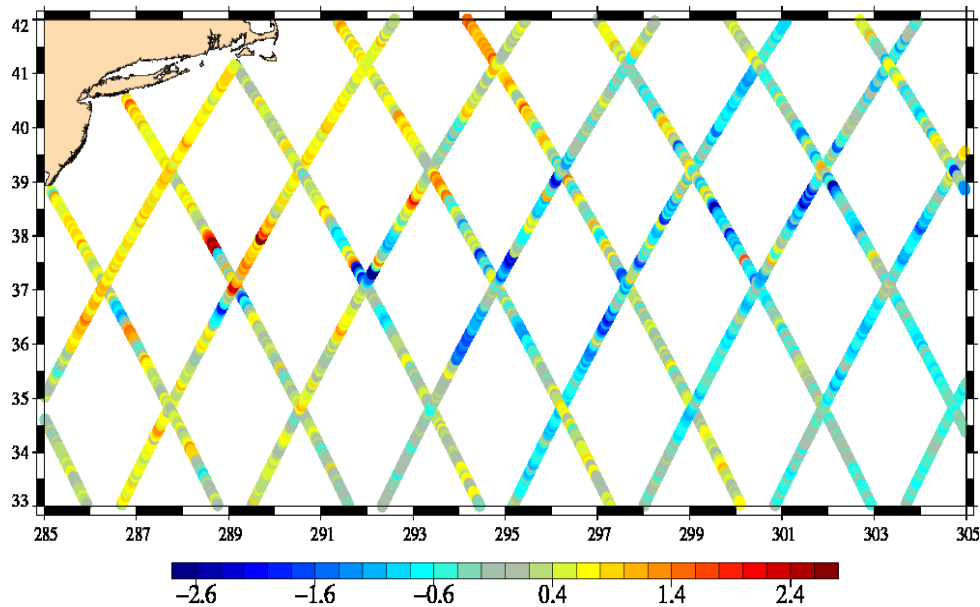


Figure 2 : Unit cm. Difference between a simple T/P average (cycles 11-268) and T/P+Jason1 average (cycles 11-353 & 11-250). Processing and standards are identical, inter-annual variability has been minimized with multi-mission maps. Regional RMS = 0.85cm.

Similarly, simple time averages assimilate any inter-annual variability at all scales. Even at global scale, and assuming the global mean sea level increases by 3mm/year, the difference is far from trivial. A simple average computed on 1993-1999 and a simple average computed on 1993-2010 would differ by more than 1.5cm for the global mean! At regional scale (Figure 3, bottom), the signal can be as large as 8cm for wavelengths ranging from 200 to 500km and still more than 2 - 3 cm for larger scales.

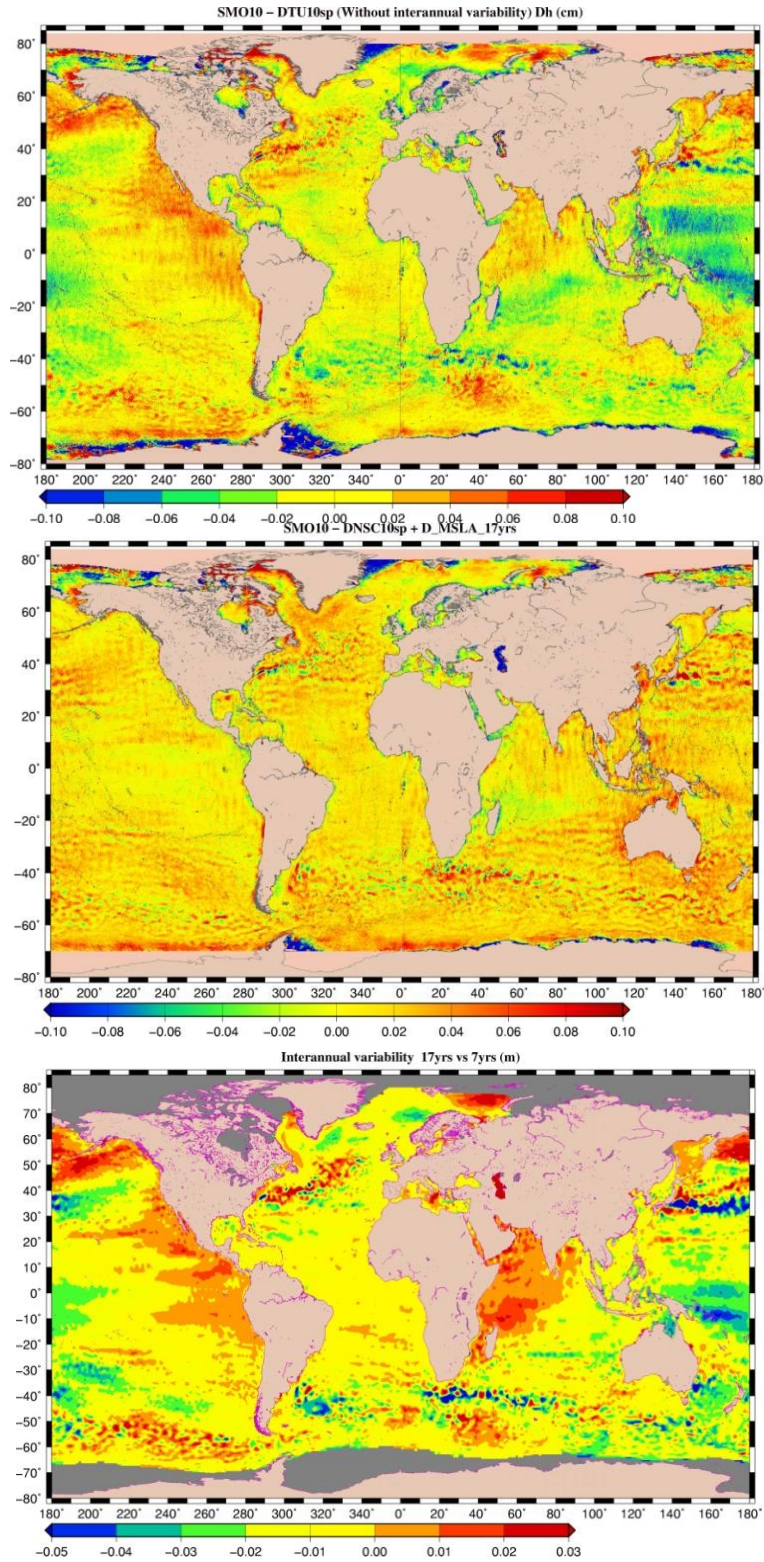
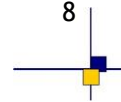


Figure 3 : Differences (m) between DTU10 and CLS/ CNES10 before (top) and after (middle) inter-annual oceanic variability is minimized with the difference between a 17 year average and a 93-99 average from DUACS multi-mission maps (bottom map).



To minimize residual errors from #A and #B, the modern computation of Mean Profiles does not use simple temporal averages (Le Traon and Dibarboure 2004). It is more complex with an iterative process where oceanic variability is minimized from the SSH using a priori knowledge from Sea Level maps derived from previous iterations or from other missions, inter-annual discrepancies are also accounted for (e.g. the GFO MP is computed on 2000-2006 but referenced onto 1993-1999 for the sake of coherency with other missions). To that extent, residual errors from #A and #B are largely non-existent on modern MSS.

2.3. Error terms #C : geophysical corrections

The main difference between the repeat track analysis and the geodetic proxy is that Mean Profiles $\langle \text{SSH} \rangle$ contain the static fraction $\langle \varepsilon \rangle$ of any error ε affecting the sensor's SSH. Conversely, gridded MSS are coherent 2D fields built from heterogeneous altimetry errors.

The error $\langle \varepsilon \rangle$ is not trivial: a two year average of Jason/ENVISAT differences exhibits 2 to 3 cm signatures with 300km to 2000km wavelengths (Ollivier et al, 2010). The error ε depends partly on standards and processing used (e.g. orbit solution, geophysical correction, instrumental drift and offset minimization). For example the difference from GDR-A to GDR-B is roughly 3.5 cm RMS for wavelength larger than 50km (estimated from SSHA and crossover variance reduction from A to B), and the difference from GDR-B to GDR-C is 1 to 3 cm RMS.

Gridded MSS contain an average of the residual error from all missions and thus only a fraction of $\langle \varepsilon \rangle$, plus a fraction of the error from different sensors.

Trying to better estimate the variance and covariance of $\langle \varepsilon \rangle$ - a non trivial issue- is the objective of section 3.

2.4. Error term #D: cross-track geoid gradient

Altimetry satellites generally use repeat orbits: after 10 to 35 days, the sensor flies over the same locations. But the satellite ground track is not perfectly controlled and it is often kept only in a band about 1km wide. To build time-series and

temporal references, it is necessary to use an arbitrary (or theoretical) track for the co-location process. SSH measurements are then projected onto exact co-location points. Precise cross-track projection and/or interpolation schemes are required to avoid errors of 1 to 3 cm (e.g. geoid signal blurred, interpolation or high-frequency errors and noise). Dorandeu et al (2003) also showed that this process required a good knowledge of the local cross-track geoid gradient (CTGG) to avoid an error of 2 to 3cm RMS. The CTGG knowledge was acquired during the first years of “historical” tracks: TP/Jason and the associated tandem track, ERS/ENVISAT and GEOSAT/GFO. This error is non-existent for repeat track analysis products.

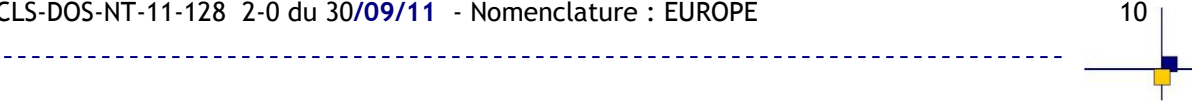
However, uncharted ground tracks (e.g. ENVISAT extended phase, Jason-1 Extension of Life phase, Sentinel-3, possibly Jason-CS) do not benefit from this knowledge, so a proxy must be used until the CTGG is computed. The best alternative is to use the local cross-track slope from a gridded MSS. In practice, the proxy is accurate only along known tracks. Away from these charted tracks, this error term falls in the #E to #I categories as it is stemming from an error of the gridded <SSH> proxy.

2.5. Errors E to I

Knowing that gridded MSS are built from Mean Profile data plus less precise SSH data from geodetic phases/missions, the minimum MSS error is the Mean Profile error: it is impossible to have a gridded MSS more coherent with instantaneous SSH than a profile specifically computed to ensure this coherency. But one could legitimately wonder why would a gridded MSS be less accurate than repeat track profiles.

There are essentially 4 types of additional errors on gridded MSS that will be analyzed in the following sections (see Table 2 for the <SSH> error overview):

1. Error #E: To ensure a global MSS coherency between all datasets, the gridding process is basically averaging all sensor-specific < ϵ > errors and especially geographically correlated ones. Consequently, not only is the gridded MSS unable to cancel the static < ϵ > error from the mission processed but it can ingest the static errors from other missions.

- 
2. Error #F: The gridding process is not able to resolve all Mean Profile scales in an isotropic way so it has to perform some smoothing to make up for signals which cannot be resolved away from known tracks.
 3. Error #G+H: The omission error is sometimes (and incorrectly) assumed to be the dominant MSS error away from known tracks, as only geodetic data are available in crossover diamonds of repetitive tracks.
 4. Error #I: Which leads to the tricky use of geodetic datasets in MSS gridding. Contrary to repeat Mean Profiles, geodetic data contain the full extent of oceanic variability, and not just the mean sea surface height content one would like to absorb in a gridded MSS. Although it is possible to minimize the MSS corruption by oceanic structures in geodetic data, handling the residual error is far from trivial.

These MSS error terms are hard to quantify separately as we don't have any dataset that would be independent, trustworthy, and long enough to build <SSH> on uncharted tracks. It is still possible to perform many analyses to quantify the order of magnitude of the sum of multiple errors after a proper band filtering. Since error estimates are linked it is not possible to perform the sum or RSS of each estimate, let alone a precise absolute error characterization of the gridded MSS. Thus, the objective of the following sections is to provide an approximate error range of the gridded <SSH> proxy.

Two approaches can be used to quantify the error: internal coherency tests (section 2.5.1) and comparison of independent datasets (section 2.5.2). The formers are based on the relative comparison of metrics derived from the exact same datasets (e.g. difference between a gridded MSS and the profiles that were used in the gridding process) and more importantly on the same database (editing, standards, pre-processing, mesoscale minimization, inter-annual signal reduction, cross-calibration between sensors...). The latter is a comparison of gridded MSS from different groups, derived from heterogeneous processing and datasets. To that extent, internal coherency tests yields lower error estimates, and the comparison of different MSS gives larger error estimates because it observes any dataset or processing discrepancy. Assuming that all recent MSS have an accuracy of the same

order of magnitude (same data standards, no revolutionary processing) the difference gives an approximate error level of all gridded MSS. Yet, even these error estimates are arguably still optimistic because they cannot reveal the common errors from similar original datasets & processing.

2.5.1. Internal comparisons based on CLS/CNES data

Moving from the charted T/P track to the interleaved track (before a tandem mean track was computed, and before gridded MSS ingested interleaved data) was shown by Dorandeu et al (2004) to yield a SSH variance increase (additional energy due to discrepancy between SSH and $\langle \text{SSH} \rangle$ on the interleaved track not resolved in older MSS). The global error was larger than 3cm RMS. More recently, Albain et al (2010) showed a similar variance increase associated with the orbital change of Jason-1 (also moved to the interleaved track). Applying a 100 to 500km pass-band filter to observe only error wavelengths that could not be separated from large mesoscale, the SSH variance increase is 1.3cm RMS on the CLS01 MSS.

More recent MSS from CLS/CNES (Schaeffer et al, 2010), DNSC (Andersen et al, 2008), and DTU (Andersen, 2010) now integrate interleaved T/P and interleaved Jason-1 data. Figure 4 shows the SSH variance change for old and new surfaces before, during, and after the orbit change of T/P. The SSH was pass-band filtered to focus on large mesoscale. The 1.3cm RMS increase on CLS01 is reproduced with recent standards. It gives a relative estimate of the omission error of the MSS on uncharted tracks (not an absolute precision number). For more recent surfaces the SSH variance increase is reduced (DNSC08) or removed (CLS/CNES10) which demonstrates that ingesting interleaved data on recent MSS improved their precision to the level observed on the historical track.

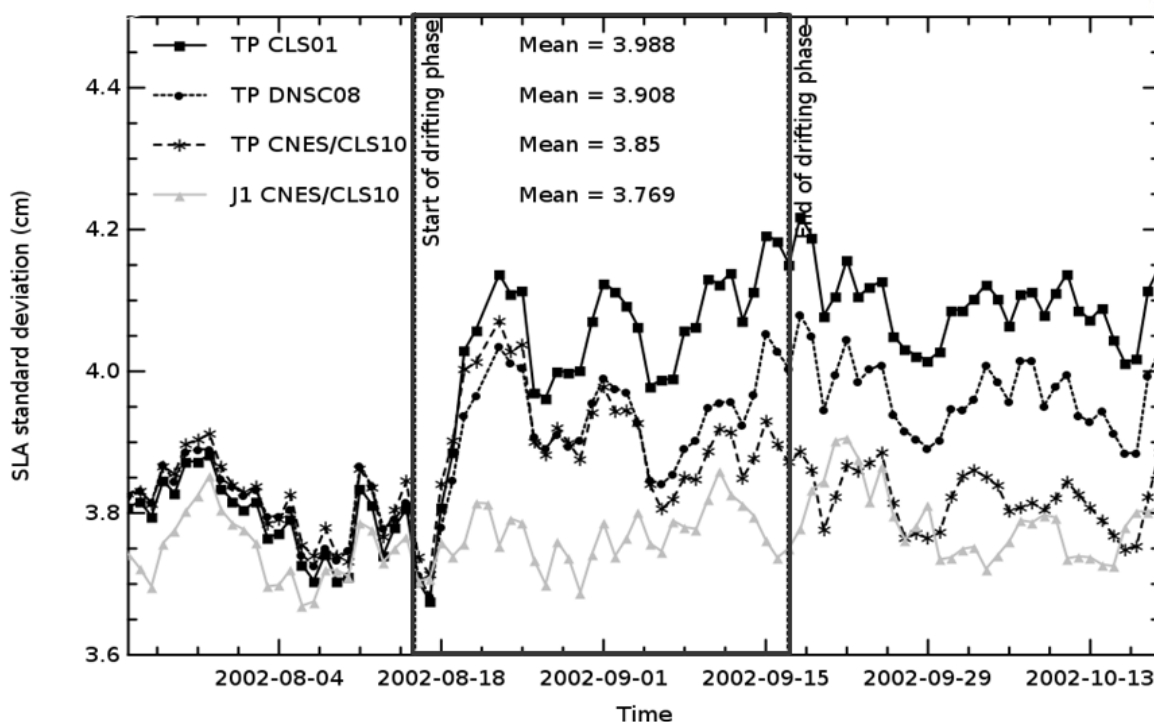


Figure 4 : Error H+I. Standard deviation of the along-track sea surface anomaly (cm) from T/P and Jason (pass-band filtered from 100km to 500km), before, during and after the orbit change.

Furthermore, the drifting period gives an estimate of the residual omission error between the historical and the interleaved track. The drift is short (one month only) and the period where T/P is neither close to the historical track nor close to the interleaved track is even shorter. Furthermore daily estimates contain a significant amount of ocean variability. Yet the SSHA variance increase is visible as a bump during the second half of August 2002. Comparing the SSHA standard deviation based on CLS/CNES2010 for both Jason-1 (historical track) and T/P (drifting) yields a maximum variance increase of up to 1.5cm rms. Over the entire period, the error is smaller (0.8cm rms). This gives some insights on the relative error increase from a gridded MSS on a charted track, to drifting data, after a pass-band filtering focusing on large mesoscale. This error is a mix of #H (omission error for large mesoscale) and #I (commission error of the MSS due to the absorption of mesoscale from geodetic data).

To quantify the errors #F, #G and #I for shorter scales, a different approach is used. Figure 5 shows the differences between the along track Mean Profile of GFO and two gridded MSS: the CLS/CNES10 which actually used the GFO profile (plain line), and a CLS10ng which was computed with the same software and data except from the GFO profile which was not used (dotted line). The differences are limited to wavelengths smaller than 100km by construction.

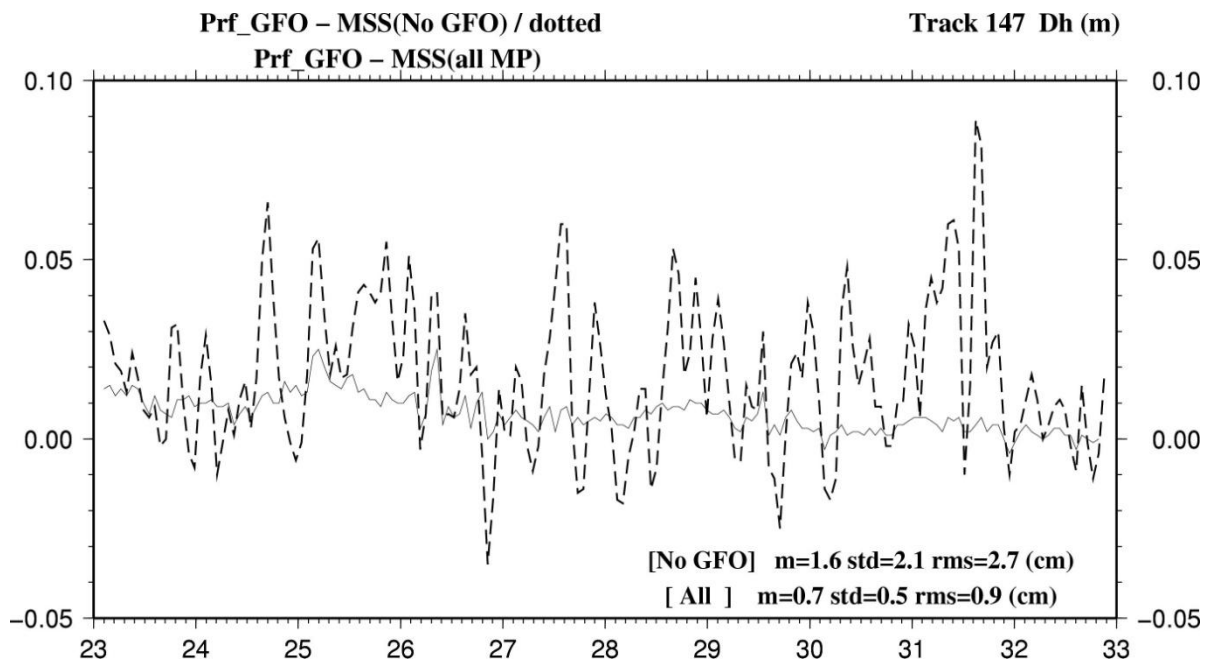


Figure 5 : Error G. Along-track difference (m) between the MPs and two gridded MSS computed with (plain) or without (dotted) the GFO dataset. Differences are limited to $WL < 100\text{km}$ by the gridding process (solution constrained by other repetitive datasets). The along-track profile is computed on GFO track #147.

Therefore, the plain line provides primarily an estimate of the small scale smoothing error (#F) along charted tracks. The error is small but not negligible (0.9cm rms). The dotted line shows what happens when the GFO dataset is taken out of the MSS. It measures the relative error (not the absolute MSS accuracy) for uncharted tracks as a sum of #I (variability from geodetic data) and #G (omission for short scales). The difference is much larger than for the plain line with a 2.7cm RMS with peaks ranging from 5 to 9 cm. Although theoretically limited to short scales, the error is not decorrelated and a smoothed version would remain coherent over 100km or

more. Note that the wavelengths affected are different from the estimate from Figure 4, so the errors stack on the total SSHA signal.

Moreover, along-track mean profiles absorb the static fraction of sensor-specific errors (section 2.5.2), and MSS need to “average and mix” such errors from all missions (#E). Thus previous figures gave only a relative error increase, and they were occulting the error term #E. To estimate how the gridded MSS absorbs correlated errors from individual missions (even on charted tracks), Figure 6 shows the residuals between the MSS and the MP used by the gridding process along the ERS/ENVISAT track. The difference often exceeds 2 to 3 cm with correlated patterns larger than 100km. This error (large scale) partly stacks with the dotted line from Figure 5 on GFO (smaller scales).

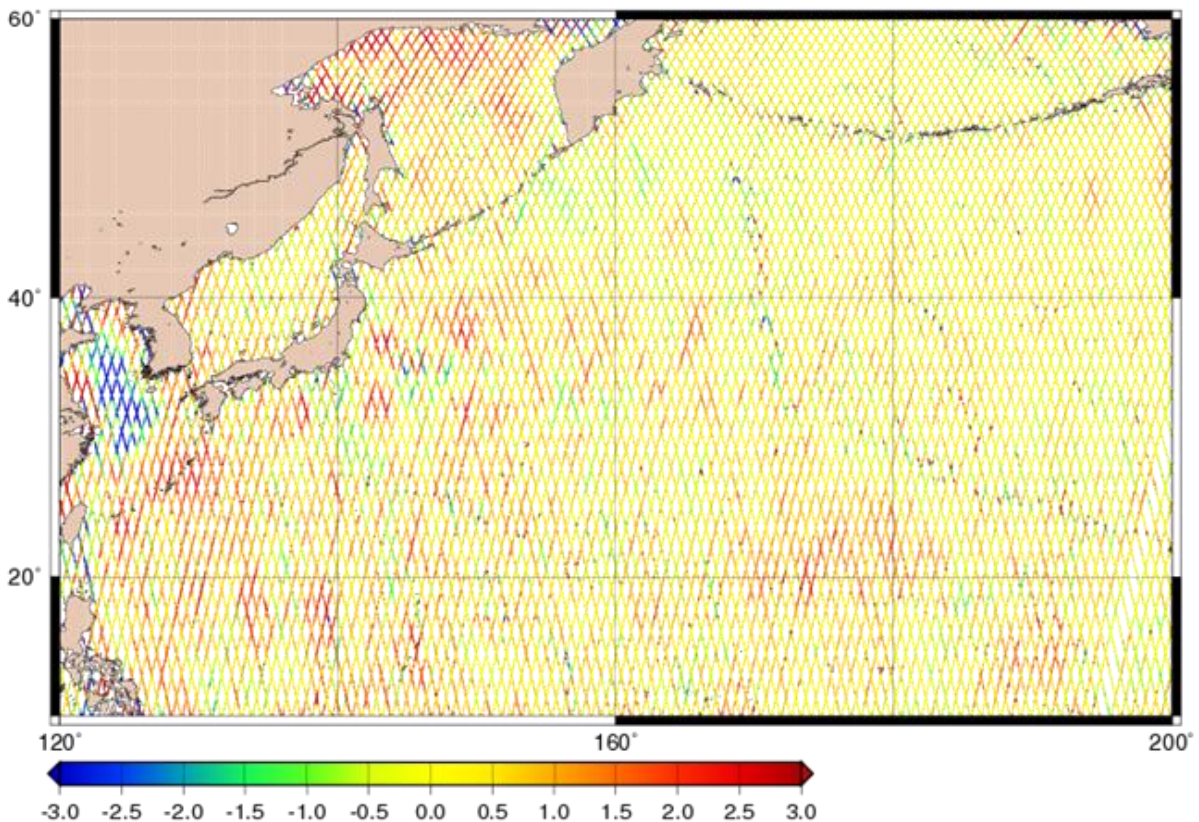
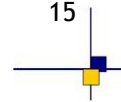


Figure 6 : Error E. Residuals (cm) between the CNES/CLS 2010 MSS and the ERS/ENVISAT mean track (data actually used in the MSS gridding).



To summarize, internal coherency tests and relative estimates point to an error level from 1 cm rms (100 to 500km) to 3 cm rms (shorter scales) if only the omission error is considered, and 2cm or more if sensor-specific residuals are taken into account. This optimistic estimate is obtained if we make the (wrong) assumption that the CLS/CNES data and processing are error-free and that the CLS/CNES2010 MSS is perfect. Conversely, if we (rightly) assume that all recent MSS have an error of the same order of magnitude, then error estimates from internal tests of this section provide only very optimistic error bars. The next section compares CLS/CNES2010, DTU2010, and DNSC08 and it provides a more pessimistic (or more realistic) estimate of the error bar as different datasets are bound to observe more data and processing discrepancies.

2.5.2. Differences between recent MSS

The top map of Figure 3 shows the difference between the DTU10 and the CLS/CNES10 surfaces. The top figure shows a simple difference of both maps. The difference is extremely large with coherent signals larger than 10cm, and signatures as large as 3 to 5 cm over thousands of kilometers. Such a raw difference is barely relevant as both surfaces were not computed on the same temporal reference. The CLS/CNES surface is referenced to a 7 year period (1993-1999) even though it uses data up to Jason-2 (inter-annual variability is accounted for through Mean Profiles as explained in previous sections). However, the DTU surface is referenced to a 17-year period.

So the bulk of the DTU-CLS/CNES difference comes from inter-annual signals. This signature is reduced using high-resolution multi-mission maps from DUACS (Figure 3, bottom). After both surfaces have been referenced on a common period (Figure 3, middle), a large fraction of the difference has been removed. The largest differences are located either at higher latitude where the DTU10 is assumed to be the most accurate (Andersen, 2010), and in the Caspian Sea. However, even in the deep ocean and at low latitudes, the MSS differences are large with 3 to 5 cm coherent signatures (200km or more). The discrepancy is even larger than 10cm in most mesoscale energetic zones.

The largest scales visible on these maps are neither due to MSS omission error, nor to smoothing, nor to a mix of sensor-specific biases. However, they could be due to

discrepancies in the data used, the standard used, the handling of inter-annual discrepancies, and the absorption of oceanic variability by at least one MSS. And since such long wavelength errors are not visible on the comparison of modern Mean Profiles computed on different time periods (see section 2.5.1 or Figure 2), any error from inter-annual or mesoscale variability would likely originate from geodetic data (and probably from GEOSAT, since ERS1 benefits from a concurrent T/P to minimize these effects). The middle map from Figure 3 thus provides a pessimistic/realistic estimate from the error term #1.

To quantify smoothing error and noise level, it is possible to look at the difference between MSS and the EGM08 geoid. Since only altimetry is able to resolve the shortest scales of the geoid at global scale, the difference to EGM08 highlights either actual geodetic features or artifacts (smoothing, background noise, outliers). Figure 7 shows a comparison of this difference over the Caribbean Sea. Although most features are similar for both MSS, in some areas (highlighted in red) the content is different. The CLS/CNES contains sharp gradients on coherent geodetic structures as expected from an altimetry-derived MSS. The DTU contains similar features albeit more subtle or less visible in an isotropic background signal. Conversely, the higher resolution of the DTU is able to better resolve some geodetic features. For short scales, the differences are far from trivial as they can locally exceed 5 to 7 cm.

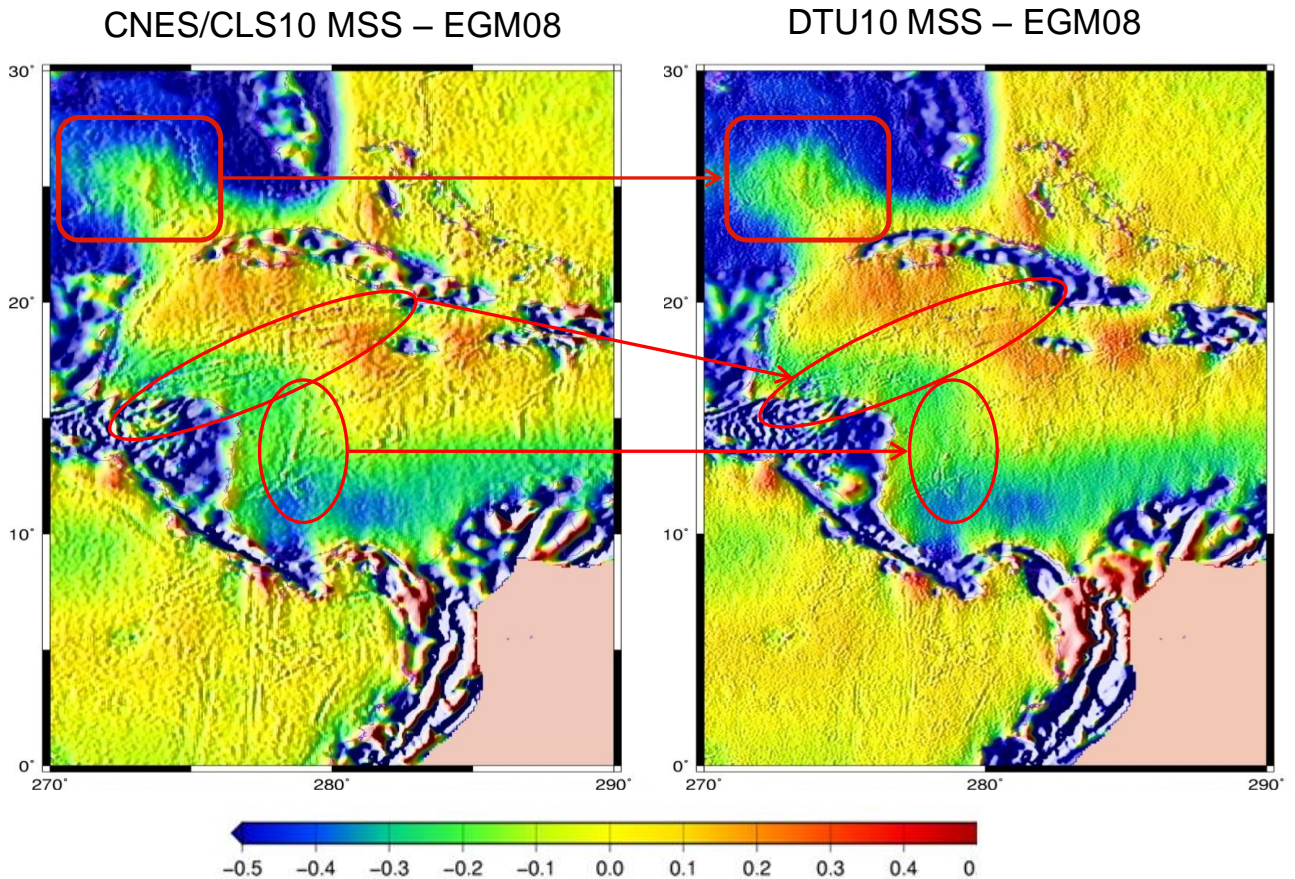


Figure 7 : Error E+F+I. Differences (m) between CNES/CLS2010 (left) or DTU10 (right) and EGM08.

Figure 8 shows a similar comparison but in a different zone (North West Pacific, over the Kuroshio Current), and after a high-pass filtering at 75km. Such high-pass filtered differences to EGM08 are expected to highlight the small-scale geodetic features visible only by altimetry. As in Figure 7, DTU/DNSC exhibits a more pronounced isotropic background signal. The lack of apparent coherency with geodetic features suggests that either this signal is background noise, or that the CLS/CNES gridding over-smoothed actual isotropic geoid signal. Assuming that both MSS have an equivalent level of error (noise on one surface, omission error on the other), this background signal is relevant to estimate the MSS accuracy at it is larger than 1cm. As in the Caribbean Sea map, Figure 8 also shows sharper gradients along bathymetric features for the CLS/CNES with differences locally larger than 3 cm.

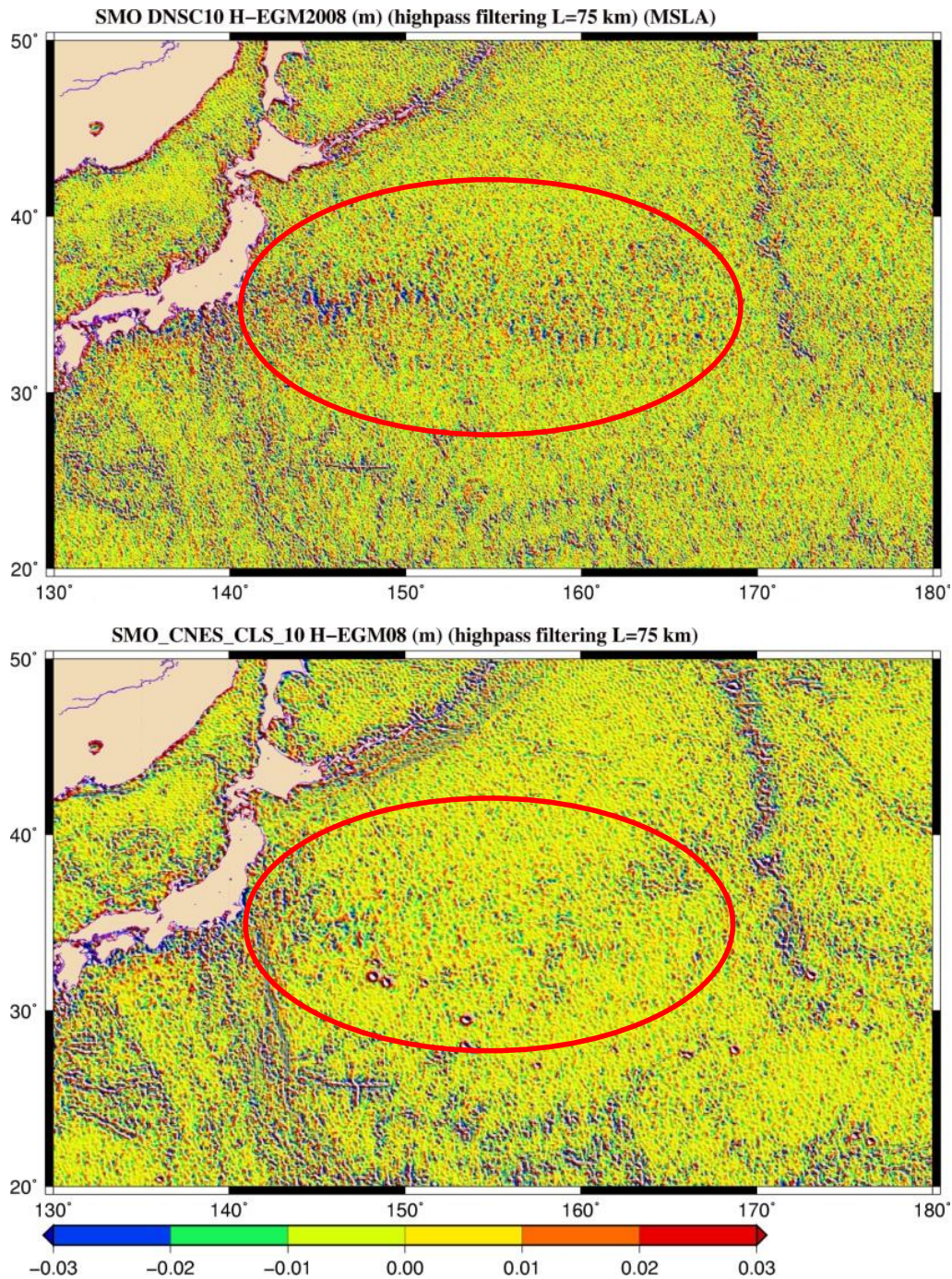
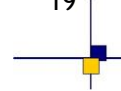


Figure 8 : Error F+H2+I2. Differences (m) between DNSC/DTU10 (top) or CNES/CLS 2010 (bottom) & EGM08 after high-pass filtering (75km).

Furthermore, in the Kuroshio Current (red ellipsis), DTU exhibits coherent differences to EGM that are larger than 3 cm. These short-scale differences between MSS and EGM are not visible on the CLS/CNES surface. At first glance, these features do not



look like coherent geoid signal, and they could be explained by mesoscale residuals from geodetic data in the DTU. This hypothesis is derived from the improvements made from CLS01 to CLS/CNES10 and shown in Figure 9. One of the major differences between both surfaces is the improved handling of mesoscale corruption of geodetic data in CLS/CNES10. The left map of Figure 9 shows an unfiltered difference between CLS01 and EGM08 with artifacts in the shape of ERS1 diamonds (the densest repetitive altimetry grid available to this day). With more input data and better mitigation of mesoscale corruption of geodetic data (only input data available within ERS1 diamonds), the artifacts disappeared (Figure 9, right). The difference between CLS01 and CLS/CNES10 (Figure 9, right) clearly illustrates that the error terms from omission (#H) and from mesoscale corruption (#I) are primarily located on short scales (as shown in the previous section).

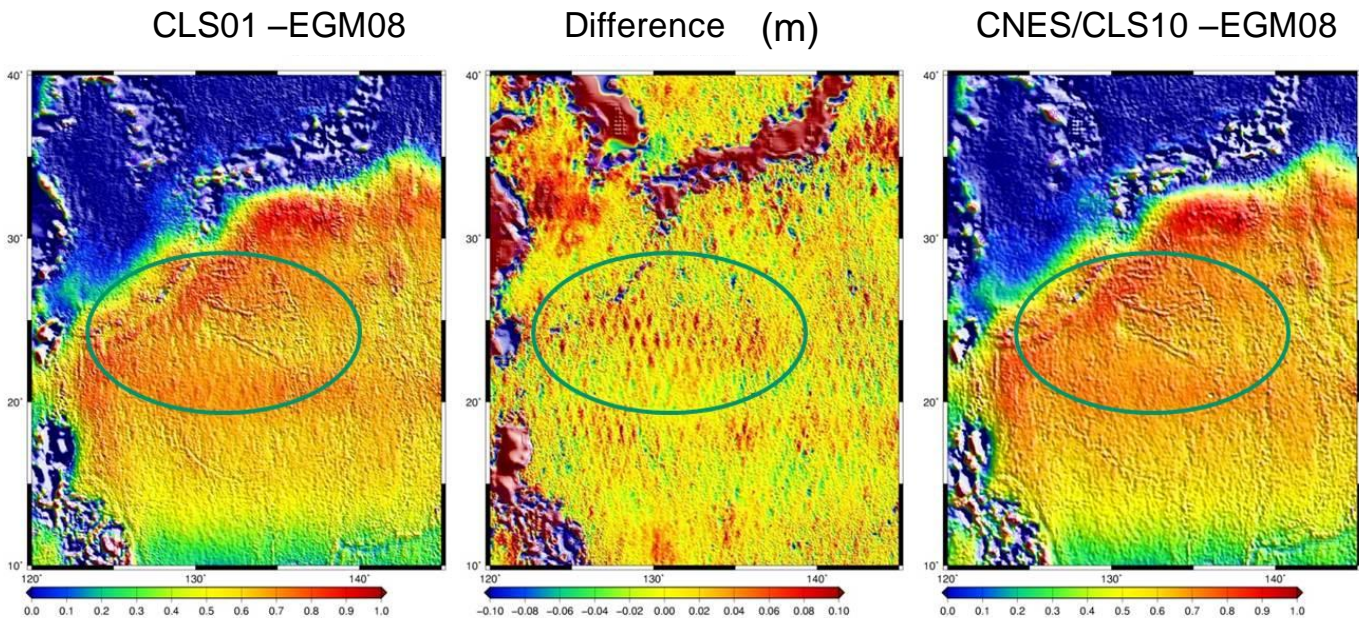


Figure 9 : Error I+H. Raw differences (m) between CLS01 and EGM08 (left), CLS/CNES 10 and CLS01 (middle), and CNES/CLS10 and EGM08 (right). Red diamonds located between ERS/ENVISAT tracks (green circles) highlight the improved minimization of mesoscale handling in geodetic data

Thus the top map of Figure 8 suggests that recent MSS still have a 3 to 5cm error at short scale, due either to corruption from geodetic data (DTU), or to over-

smoothing of actual geoid features that cannot be separated from mesoscale in geodetic data (CLS/CNES) in the area.

Indeed, the CLS/CNES 2010 mean sea surface was actually shown to contain rare outliers created by the drastic geodetic data processing (Schaeffer et al, 2010). An example of such artifacts is given in Figure 10. Two quasi-isotropic seamounts formerly resolved in the CLS01, and visible in DTU10 (Figure 10, right) were largely truncated in CLS/CNES10 (Figure 10, middle). Although the signal was visible in geodetic data from ERS1, the automated pre-processing detected and reduced an isotropic signal coherent on 50km from geodetic data, although it was clearly too large to be mesoscale in this area. A simple change in the screening process was able to remove this outlier (Figure 10, left). About 0.03% of the CLS/CNES10 points are affected by outlier of this amplitude and 0.2% for similar events of smaller amplitude. The CLS/CNES11 mean sea surface was computed using this upgraded screening process, and it is now distributed by AVISO in replacement of CLS/CNES10.

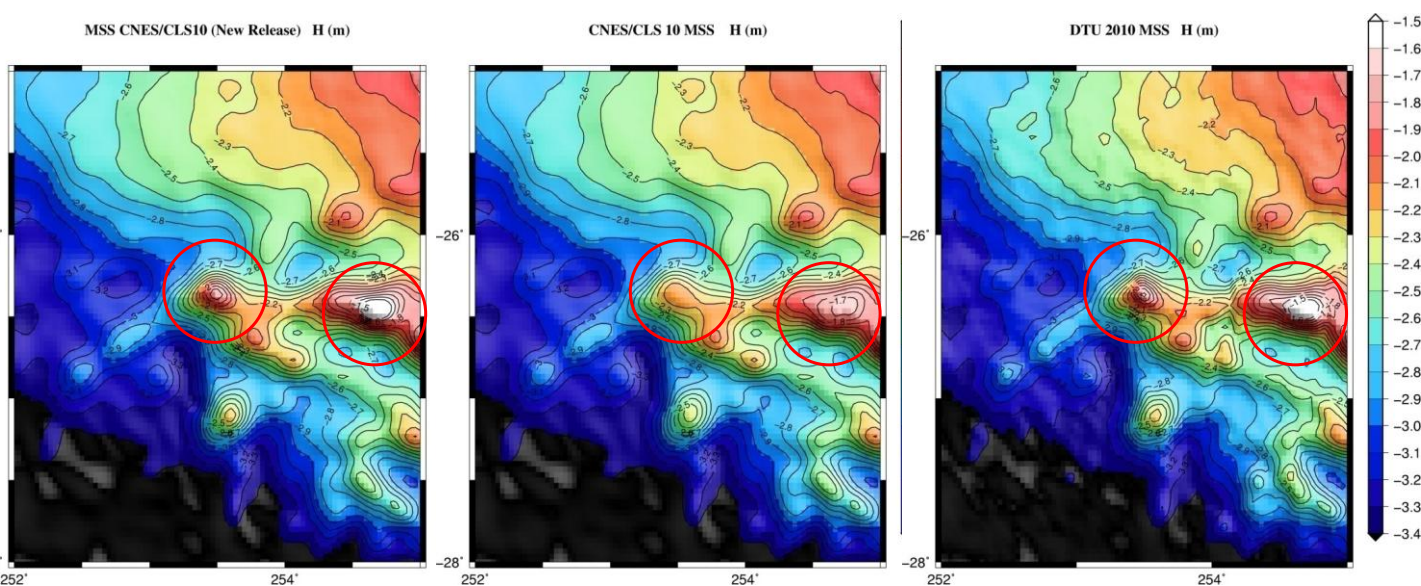
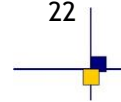


Figure 10 : Artefact created by the mesoscale minimization process from the MSS gridding process. Some rare isotropic seamounts that were correctly resolved by the CLS01 MSS or the DTU10 (right) were smoothed in the CLS/CNES10 (middle). A change in the CLS/CNES10 gridding process can restore the original information from geodetic data (left).

To summarize, the comparison of different surfaces based on different data and processing yields a much larger error estimate if we assume that each surface contains independent error sources. Even after inter-annual discrepancies are removed, mean sea surfaces exhibit discrepancies ranging from 3 to 5 cm for large mesoscale wavelength, and locally more than 5 cm for shorter scales, with rare outliers larger than 10cm. Furthermore the distribution of the error is neither random, nor gaussian, and global RMS values largely underestimate the extent and the spatial coherency of the largest MSS errors, let alone rare local outliers.



3. ESTIMATING THE CONTRIBUTION OF GEOPHYSICAL CORRECTIONS UNCERTAINTIES IN THE MSS VARIANCE AND COVARIANCE ERROR BUDGET.

3.1. Impact of range and geophysical correction errors.

In this section, the impact of using different range and geophysical corrections on multi-years MSS determination is assessed with the aim of developing error characteristics for the range and geophysical related error contribution to the total MSS error, corresponding to the $\langle \epsilon \rangle$ term discussed in section 2.3.

The following range and geophysical corrections applied for the derivation of the following available MSS models.

Standards	CLS01	DNOSC08MSS	CLS10	DTU10MSS
Reference period	1993-1999	1993-2004	1993-1999	1993-2010
Orbit	ORB_POE_N	GGM02/ITRF2000	ORB_POE_N	EIGEN-GL04C
Dry troposphere	ECMWF	ECMWF	ECMWF	ECMWF
Wet troposphere	Radiometer	ECMWF	Radiometer	Radiometer
Ionosphere	Altimeter	Altimeter	Altimeter	Altimeter
Dynamic Atmosphere	IB (1011 mbar)	IB (1013 mbar)	MOG-2D_IB	MOG-2D_IB
Ocean tides	GOT 99	GOT 00.2	GOT4.7	GOT4.7
Sea State Bias	BM4	BM4	Non-PARAM	Non-PARAM

Table 3: The set of range and geophysical corrections applied for CLS01, CLS10, DNOSC08 and DTU10MSS. Only corrections applied to the TOPEX/Poseidon and Jason-1 have been shown. The corrections applied to different satellites missions (ERS1, ERS2, GEOSAT, GFO etc) included in the determination of the MSS will be different

Most range and geophysical corrections are more or less equally accurate in the deep ocean in terms of reducing the variance of the sea surface height. The accuracy of the models used to compute the range corrections, is naturally important for both the development of sea level anomalies and the determination of the mean sea surface. However, it is equally important to know if the corrections have a different mean value over time as this will directly propagate into the MSS error.

This is because the MSS is derived by combining data from temporal average of several years of highly accurate exact repeat mission (ERM), with data from the older non-repeating geodetic mission (GM) like ERS-1 and GEOSAT.

Consequently the error in the range and geophysical corrections enters the computation of the mean sea surface in two ways. First through the temporal averaged error of the range corrections as these are used to determine the mean profiles. Secondly, the error in the range corrections directly enters the computation of the MSS through the non-repeating geodetic mission data. The latter is very difficult to quantify as the geodetic mission tracks are normally fitted onto the mean profiles (i.e., Andersen and Knudsen, 2009) to suppress long wavelength signals (typically longer than 300 km) leaving only short wavelength signals. Consequently this fitting will also reduce long wavelength range correction errors leaving only short wavelength part of the range correction errors.

There is unfortunately no easy way to quantify contribution to the MSS error and the best way is to use the interpolation error as a proxy for this error. This will be the scope of another section.

The scope of this section is to quantify the temporal averaged error of the range corrections as these are used to determine the mean profiles. These errors can convenient be studied/approximated through investigation of the most up to day corrections used on recent MSS models (see Table 3). The following set of state of the art range and geophysical correction models will be studied to access the error characteristics.

	Corrections
Dry Troposphere	ECMWF (Model) NCEP (Model)
Wet Troposphere	Radiometer (onboard) ECMWF (Model)
Ionosphere	Smoothed Dual Frequency Radiometer IRI 2007 (model)
Dynamic Atmosphere Correction	IB (Model, Local pressure) MOG 2D Model
Tides	FES 2004 (Model) GOT 4.7 (Model)
Sea State Bias	BM4 (model) CLS NPARAM-GDRC (model)

Table 4: The state of the art range and geophysical corrections.

The analysis is performed by comparing different (but simultaneous) mean profiles for which alternative corrections are applied. The mean profiles considered are the following:

- 6 years (2003-2008) mean profiles for Jason 1 (cycles between 36 and 256)
- 6 years (2003-2008) mean profiles for Envisat (cycles from 13 to 74)

Below the root squared sum (RSS) of the differences of all six corrections are shown in order to illustrate how the use of sun-synchronous satellite affects the computation of mean values. The RSS of all corrections is shown in the same color scale for the Jason-1 and ENVISAT 6 year profiles. The reason for the larger values for ENVISAT is because the ERS and Envisat satellites are sun-synchronous. Consequently, sun-synchronous contributions to the range and geophysical corrections will be observed at the same phase and averaging the satellite altimeter observations over time will not average them out. As such these sun-synchronous contributions might end up in the sea level anomalies. However, for mean sea surface computation it is important to include the sun-synchronous satellites ERS and Envisat as these are the only satellites covering the high latitude regions between the 65 and 82 parallels and because these satellite have a 3.5 times denser groundtrack pattern compared with Topex and Jason. In order to circumvent the increased error on the sun-synchronous satellite the ERS/envisat mean profiles are normally fitted to the TOPEX profiles in order to minimize the effect (see i.e., Andersen and Knudsen 2009).

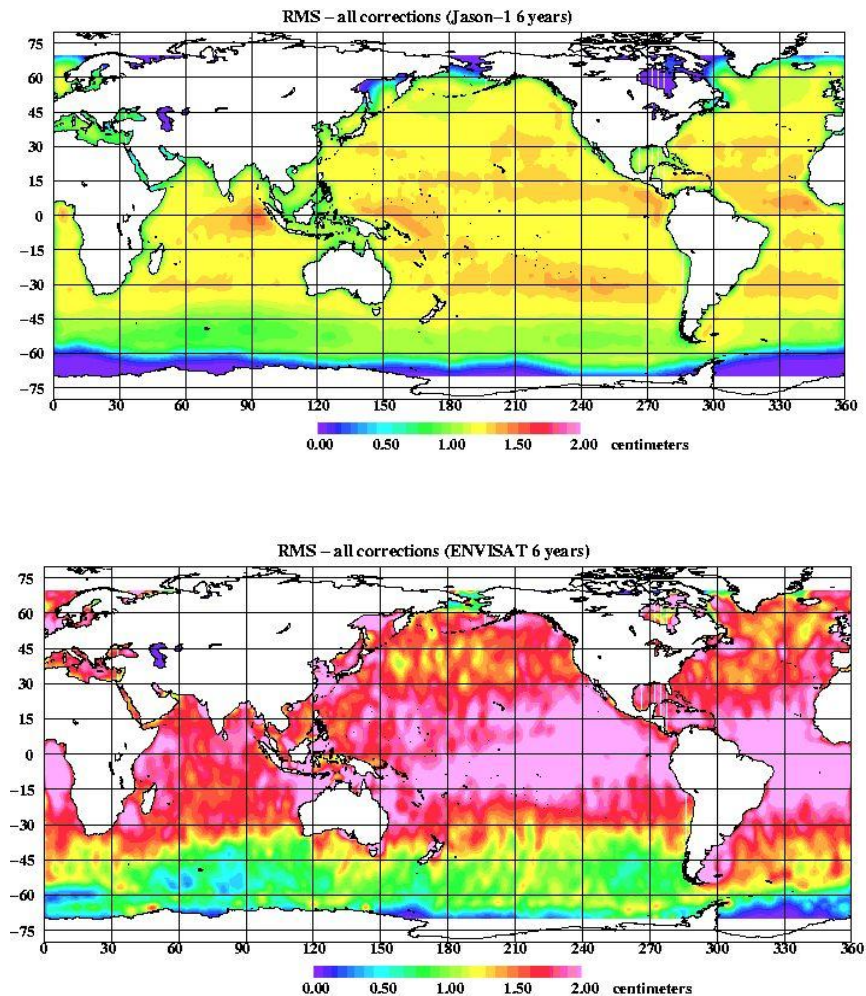


Figure 11: The root square sum of the difference between the 6 corrections shown in Table 4 and representing the largest effect of using different state of the art corrections to MSS determination.

The root square sum of the difference between the 6 corrections shown in Figure 11 represents the largest effect of using different state of the art corrections to MSS determination and as such is a conservative estimate of the effect of using different range and geophysical corrections on altimetric MSS determination. An additional small effect might arise from the inclusion of the Geodetic mission data, but this will be ignored in the following investigation.

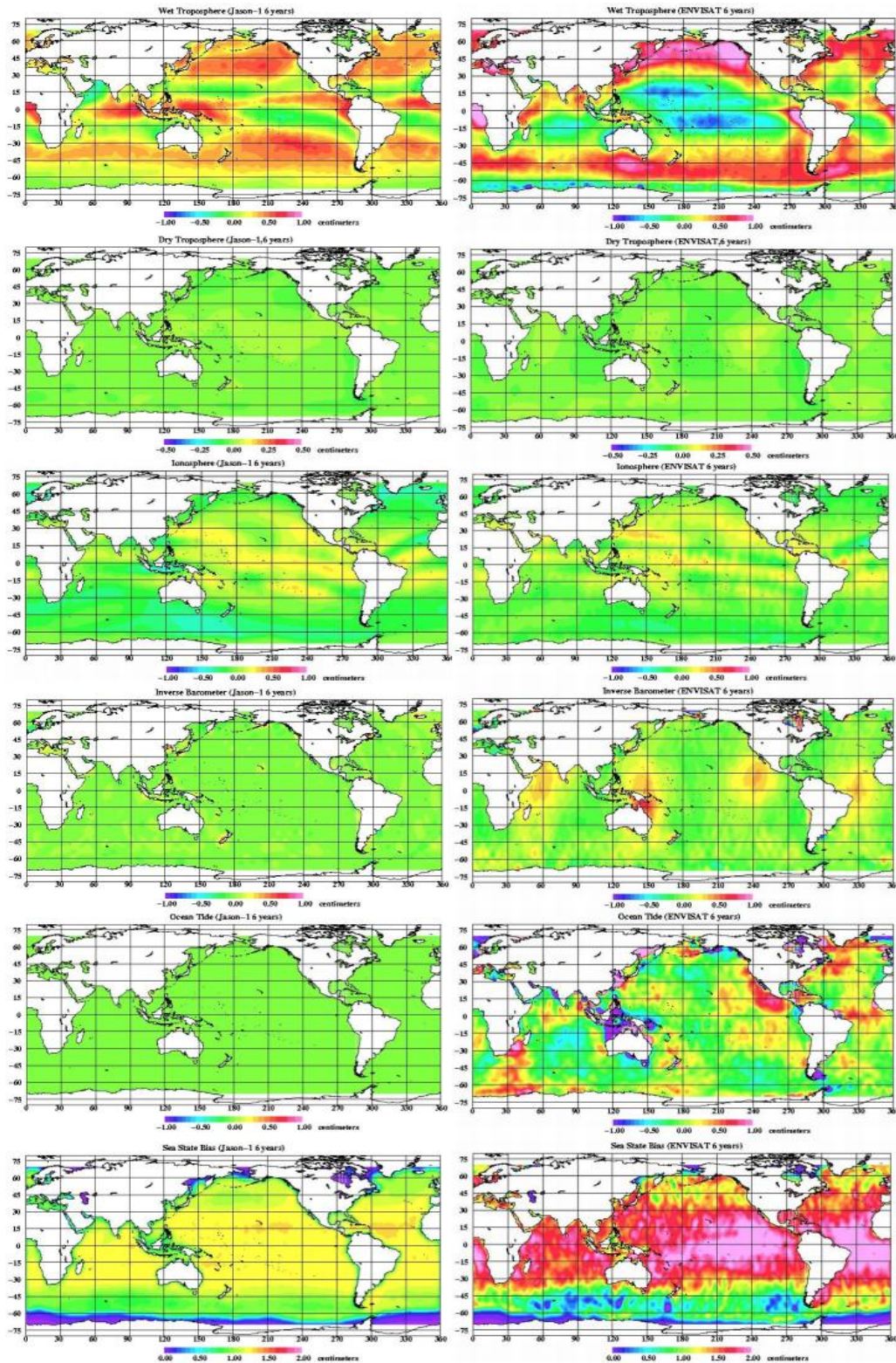
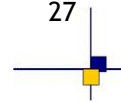


Figure 12: RMS of the difference between state of the art range and geophysical correction interpolated from six years Jason-1 profile (left) and six year Envisat profiles (right).



In Figure 12 the RMS of each range and geophysical contribution to the global RSS is shown. Notice that these plots are small and interpolated version of the plots in Rio and Andersen and for detailed evaluation these full resolution plots containing the track by track differences should be consulted. It is seen that the difference in the SSB dominates. The difference is here computed from the use of the BN4 SSB correction versus the NPARAM SSB correction. The colour scale for the difference in the SSB correction in Figure 12 and the RSS of all corrections in Figure 11 is identical for convenience. It is in the nature that this should be the largest contributor to the difference in the MSS determination as this correction is a bias correction whereas the other corrections are dynamic corrections. It is also in the nature that different ocean tide correction will have nearly no mean contribution and hence no impact on the MSS as the TOPEX satellite was designed to optimally sample the tidal signal (see Parke et al. 1987). This is not the case for the ENVISAT profiles due to the nature of the sun-synchronous orbit choice (see above)

In investigate the consistency between recent MSS models and to find out which combination of MSS models were the optimal to study error covariances of the difference between the models we performed a study which were carried out by computing point by point comparison between the models for depth greater than 50 meters were carried out and the result is shown in Table XX.4. Notice that for CLS10 a number of outliers have been detected which biases the comparison for this model. Subsequently these were removed by requiring that the absolute difference with other model should be less than 1 meter. The highest similarity was found between CLS01 and DNSC08 which is also a consequence of the fact that these two models have nearly the same averaging period. The outliers in CLS10 also meant that this model was not preferred for the comparison and investigation of error covariance functions in the following investigation.

	CLS01	DNSC08	CLS10	DTU10
CLS01	-	1.5	-	-3.3
DNSC08	3.9	-	-1.1	3.0
CLS10	-	23.2 (5.4)	-	2.8
DTU10	4.2	-	23.4(5.5)	-

Table 5: Mean and standard deviation between recent MSS models. The values above the diagonal is the mean difference in cm. The values below the diagonal are the standard deviation between the models in cm. The numbers in brackets are the standard deviation once outliers > 1 meter has been removed

Empirical covariance functions were calculated over 20° by 20° regions globally for each 2° by 2° latitude by longitude creating global sets of covariance functions. The spatial error variance averaged over these blocks and the correlation length (where correlation reaches 0.5) is shown in Figure 13 and Figure 14.

There will be an issue with the computation in coastal regions. In order to enable computation closer than 10° from the coast the data were interpolated and smoothed onto the coast to limit coastal effect on the covariance function. This still means that a coastal boundary zone of several degrees should be considered in the computation.

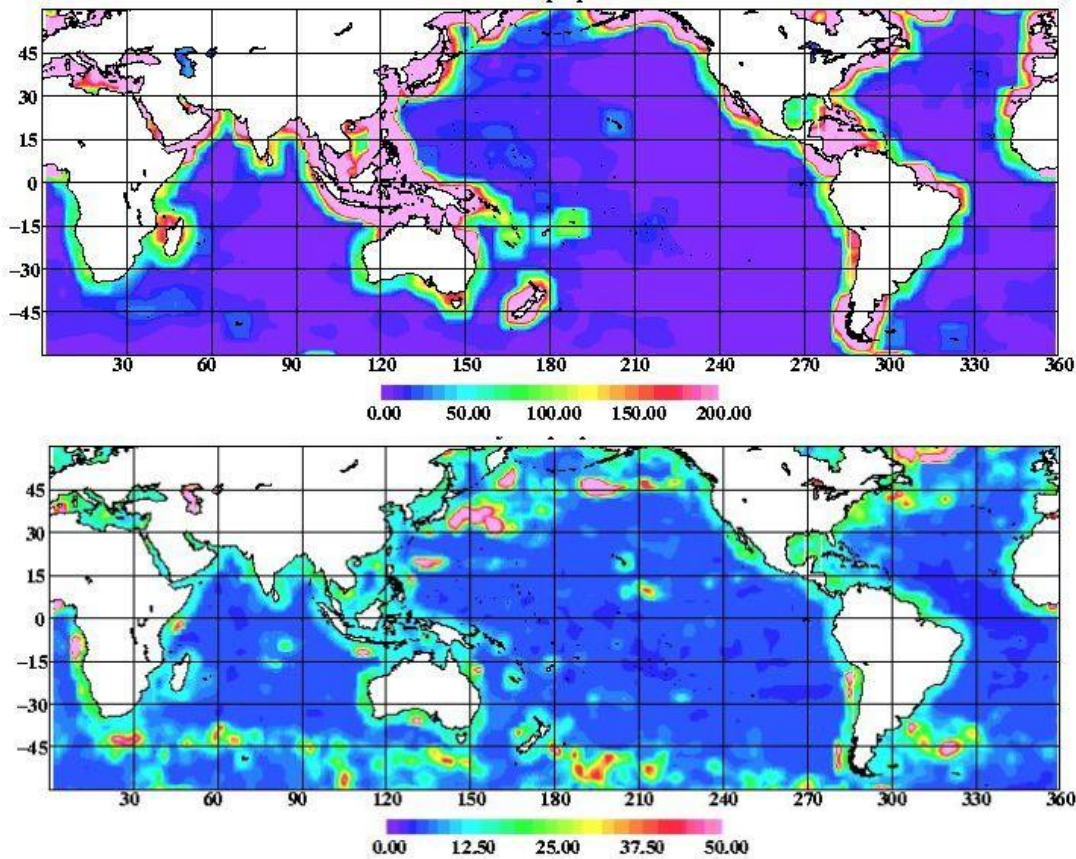


Figure 13: Spatial error variance computed from the difference between the two most recent independent MSS models. The CLS01MSS and the DNSCO8 MSS. The upper figure shows the error variance associated with the difference (in cm^2). The lower figure shows the correlation length of the "error" The difference between the CLS01 and DNSCO8 MSS used for this computation is shown in Figure 16

Using the difference between the two most recent independent MSS models (the CLS01 and the DNSCO8) only acts as a crude proxy of the accuracy of recent MSS models, but it provides important information on the error structure that is investigated below. The correlation lengths shown in the lower panel of Figure 13 indicate that the difference and most likely the error is dominated by short wavelength features in the deep ocean where the error is the smallest according to the upper panel of Figure 13. Consulting with Figure 16 below this indicates that the track related errors most likely related to smoothing of the data. The error related to the smoothing was described in more details in the previous section, but the difference between the smoothed MSS and the mean profiles often exceeds 2 to 3 cm with correlated patterns larger than 100km in the north-south direction.

A close inspection of Figure 13 also indicates that at shallow water / closer to the coast the error increases and changes to longer wavelength. This means that the error gets dominated by different signals which might typically be related to errors in the range and geophysical corrections. This is one of the issues that are pursued below.

The spatial error variance as well as the correlation length (where correlation reaches 0.5 assuming an isotropic error covariance) is shown in Figure 14 and Figure 15 for the six range and geophysical corrections. The large difference in the magnitude of the spatial error variance is clear from Figure 14. The correlation length shown in Figure 15 has typical values of 50 to 150 km but with distinct spatial pattern. Particularly the pattern of the Sea State Bias typically reflects the region where this signal is dominating the errors related to the range and geophysical corrections.

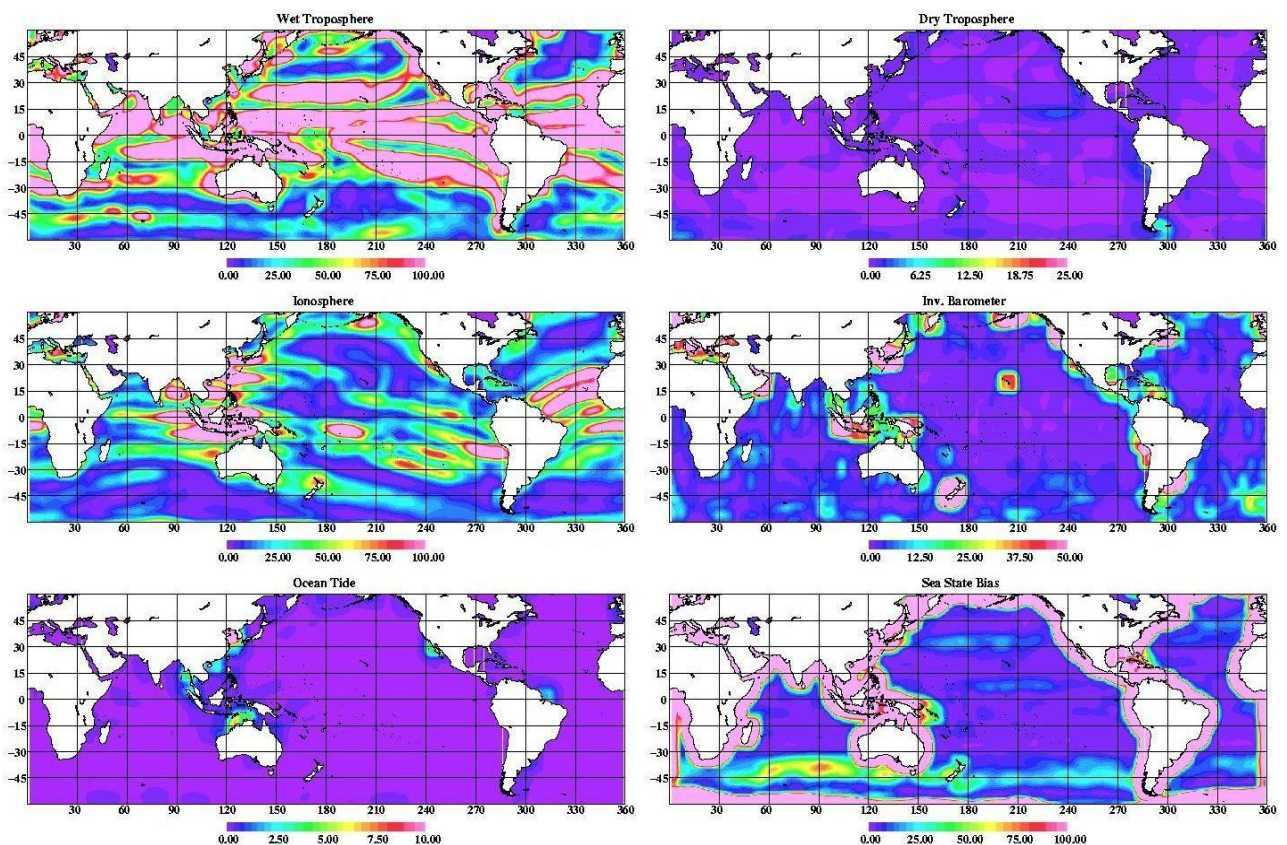


Figure 14: *Spatial error variance for the range and geophysical errors in $\text{cm}^2 \times 100$.*

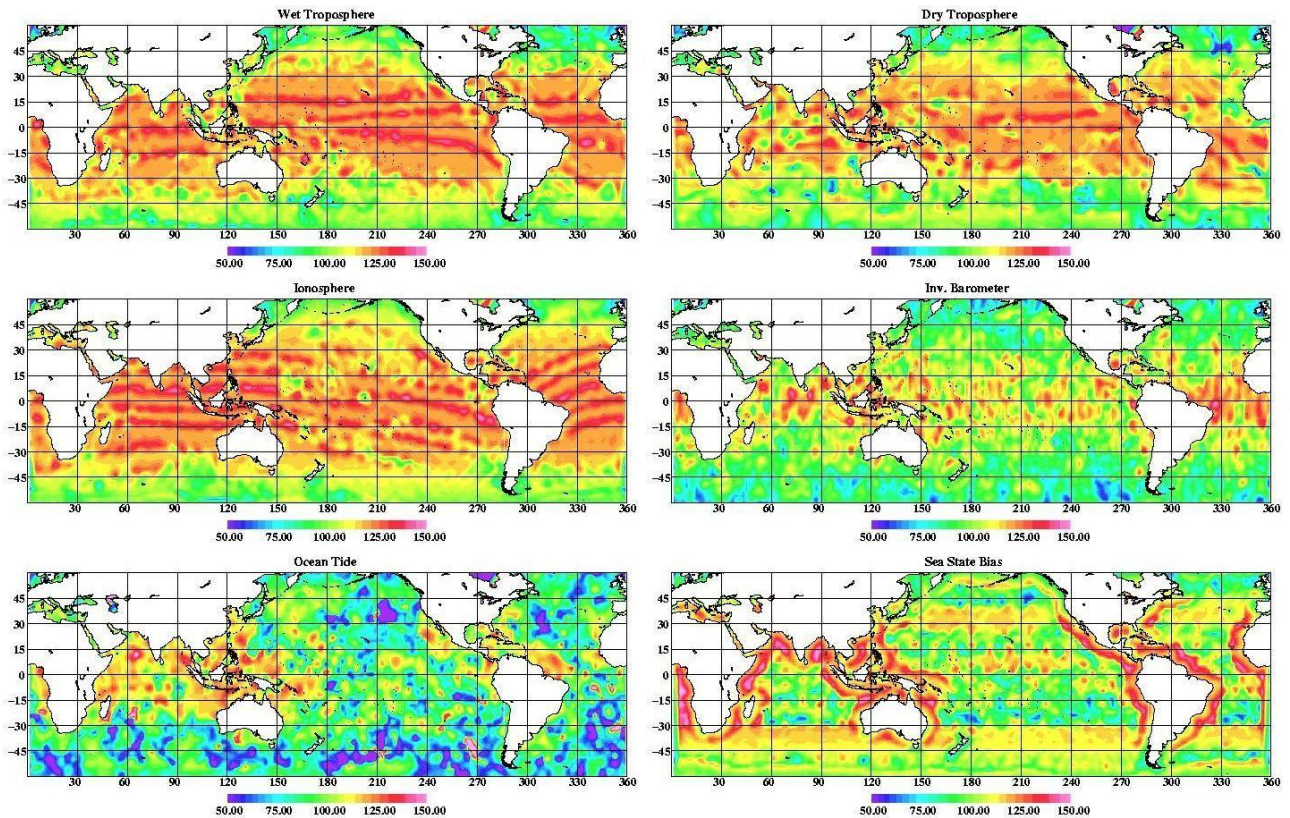


Figure 15: Correlation length in km of the range and geophysical error estimate.

3.2. Covariance functions for typical regions.

In order to further investigate the error covariance functions associated with the range and geophysical corrections four typical regions were selected. Naturally more regions could be investigated, but in the sake of limiting the number of pages and choosing the most typical regions these four regions were selected. The regions are thought to represent regions of typical ocean features and dynamics and regions at different latitudes and proximity to the coast.

The four regions are:

- North Atlantic Region (center of the North Atlantic Ocean)
- Tropical Pacific Region (Equator)
- South East Asia Region (close proximity to the coast)
- Antarctic Region (very high latitude)

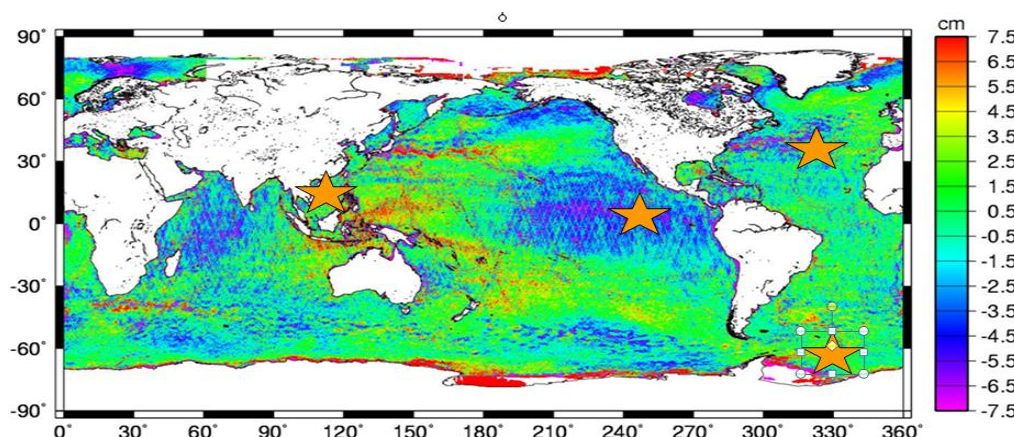


Figure 16: Location of the four typical regions selected to illustrate the different behavior of the error covariances associated with the use of different range and geophysical corrections. The underlying figure is the difference between the two most recent in-dependent MSS models (the CLS01 MSS and the DTU08MSS model) given in cm.

3.2.1. North Atlantic Region

The North Atlantic region is the region bounded by 30° N and 50° N, 30°W - 50°W and is located in the centre of the North Atlantic with depth ranging between 1 and 5 km and the Gulf Stream extension passing through its upper right corner.

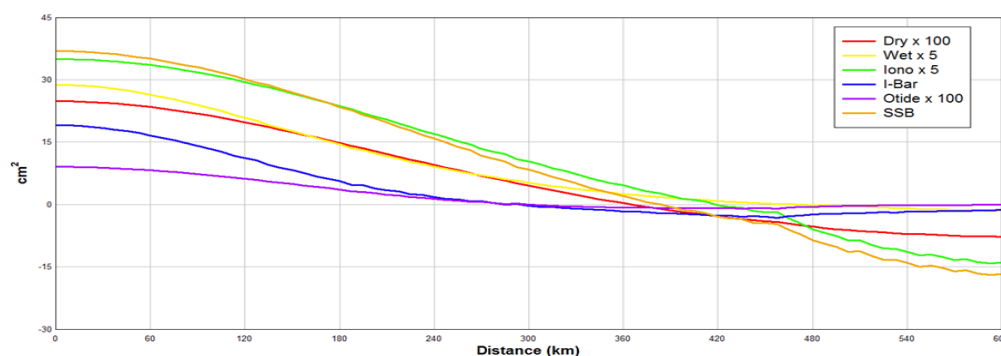


Figure 17. The covariance functions for the errors in the range and geophysical corrections for 6 year mean Jason profiles.

Covariance functions associated with the approximate errors in the range and geophysical corrections for 6 year mean difference based on Jason sampling is shown in Figure 17. Different scaling has been applied to the different covariance functions in order to plot these on the same figure. In this region the SSB dominates followed by the Dynamic Atmosphere, ionosphere and wet troposphere. The two dimensional covariance function for the six range and geophysical corrections are shown in Figure 18. Only the wet troposphere is close to being isotropic.

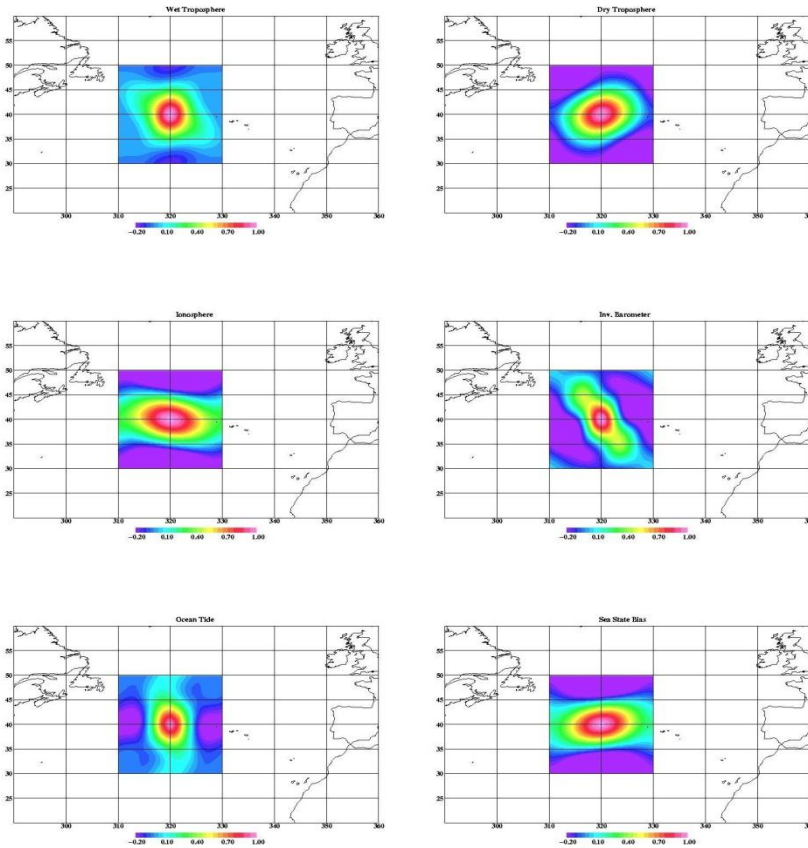


Figure 18: Two dimensional covariance function for the centre of the North Atlantic region for each of the range and geophysical errors for 6 year mean Jason profiles

In order to study if the two dimensional covariance functions determined from differences in the geophysical range and geophysical corrections along 6 years of Jason-1 observations differ from 6 years of Envisat observations, the similar covariance function are shown in Figure 19 for Envisat. There are some similarities for particularly the wet troposphere and the ionosphere, but the remaining covariance functions are very different.

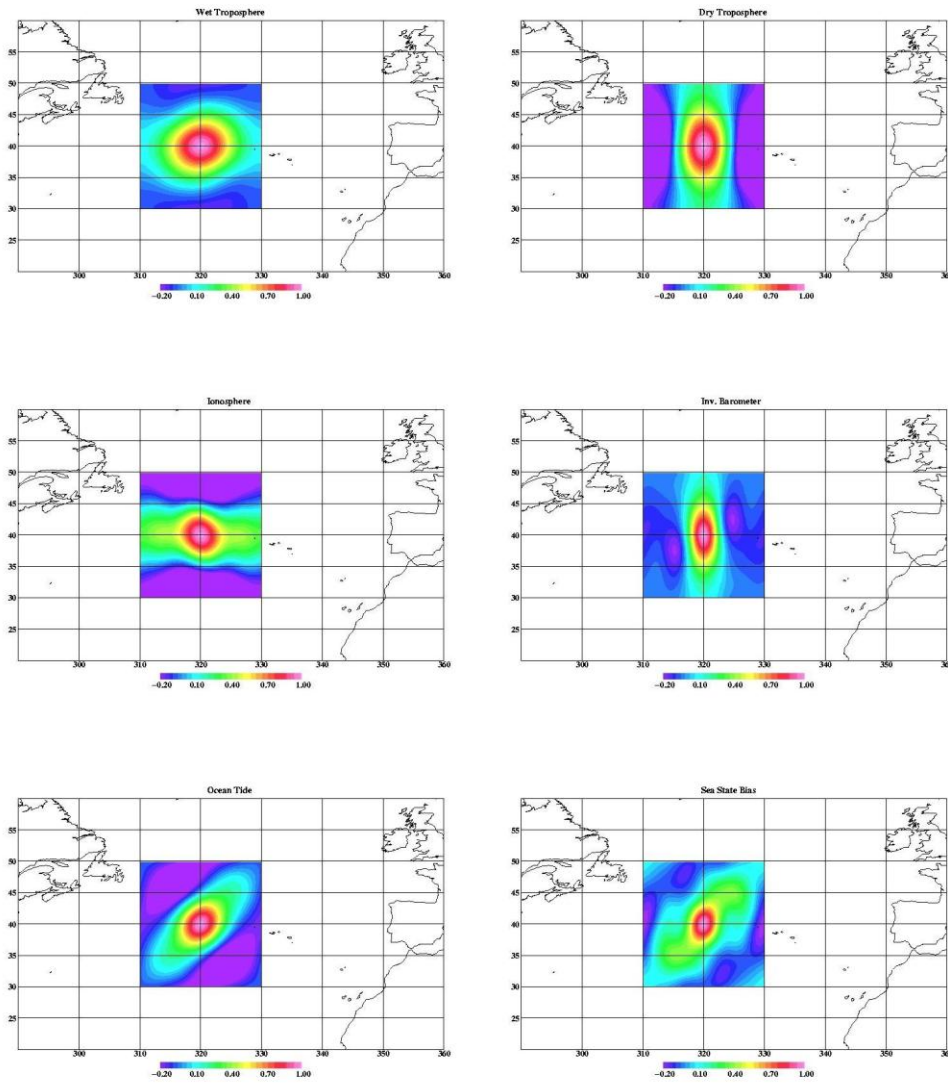


Figure 19: Two dimensional covariance function for the centre of the North Atlantic region for each of the range and geophysical errors for 6 year mean Envisat profiles

3.2.2. Tropical Pacific Region

The Tropical Pacific Region is bounded by 10° S and 10° N, 240° E - 260° W and is located in the tropical Pacific ocean where there is traditionally little sea level variability and little difference between recent MSS models as shown in Figure 16. Generally the water depth ranges between 5 and 8 km in this region.

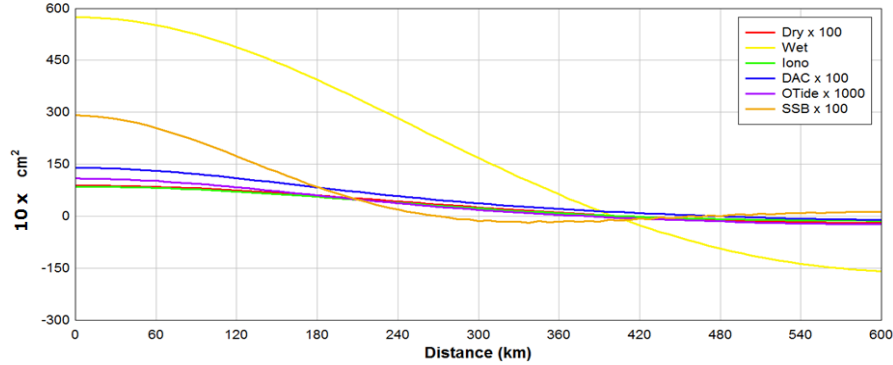


Figure 20: The covariance functions for the errors in the range and geophysical corrections for 6 year mean Jason profiles.

Covariance functions associated with the approximate errors in the range and geophysical corrections for 6 year mean difference based on Jason sampling is shown in Figure 20.

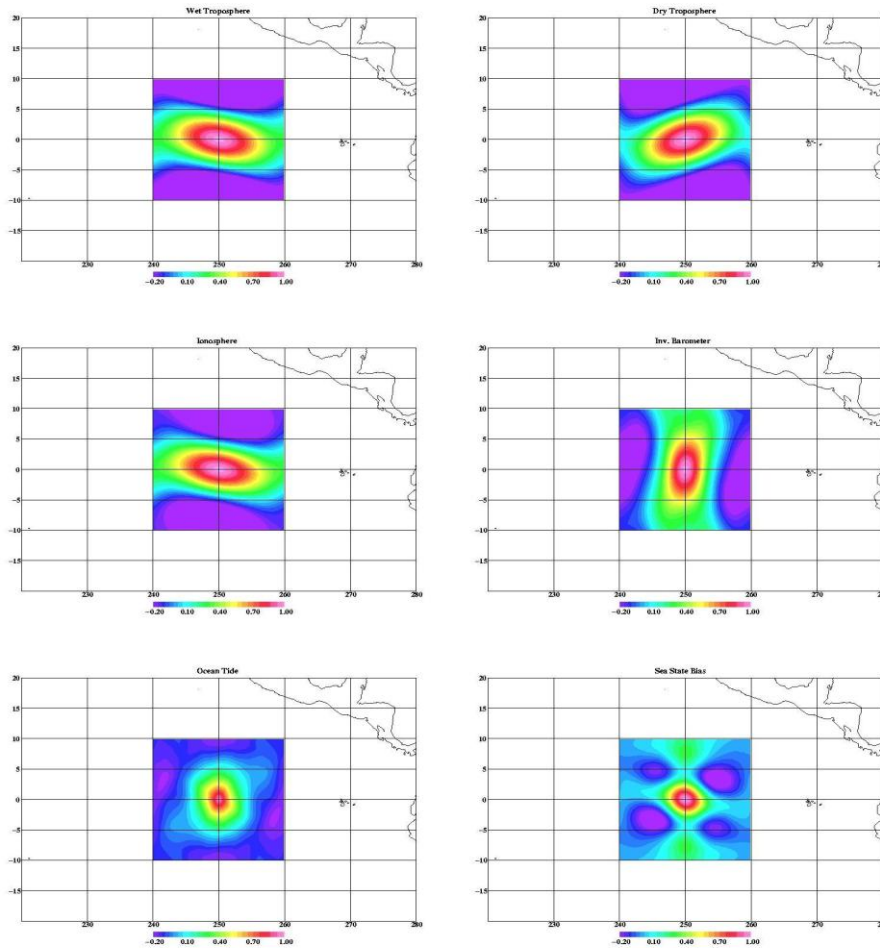


Figure 21: Two dimensional covariance function for the center of the North Atlantic region for each of the range and geophysical errors for 6 year mean Jason-1 profiles

Again different scaling has been applied to the different covariance functions in order to plot these on the same figure. In this region the errors in the wet troposphere correction clearly dominate. The contribution from the SSB “error” is relatively small. However the correlation length of this signal is clearly the shortest of all the corrections. The two dimensional covariance functions for each correction is shown in Figure 21

3.2.3. South East Asian region

The South East Asian Region is a very interesting semi-coastal region. The region is bounded by 0° N and 20° N, 105° E - 125° E and is located in the centre of the South China Sea with depth ranging up to 3 km. The 20° by 20° region could not be placed without partly including some land regions in Indonesia and other countries where the corrections were extrapolated onto land using smooth extrapolation.

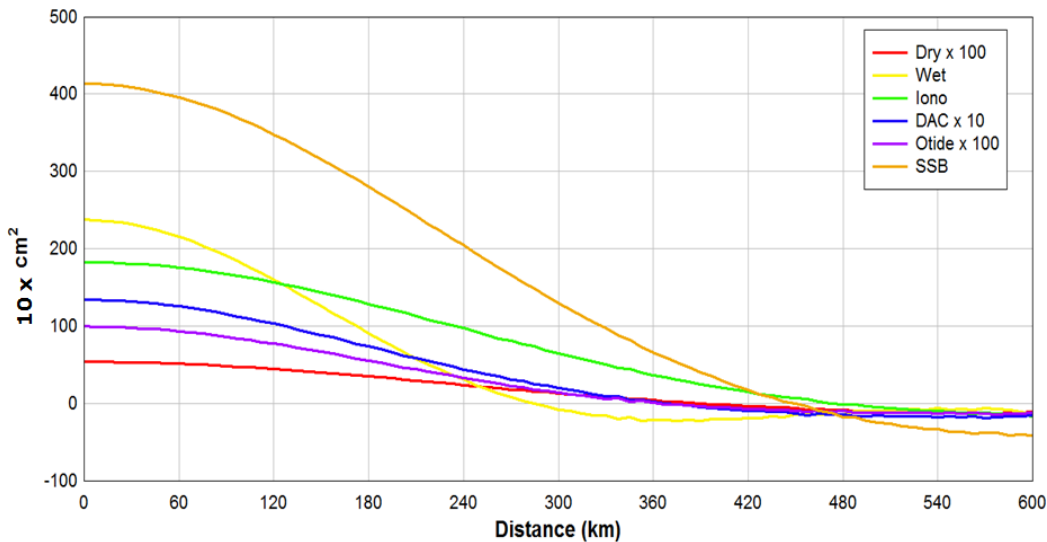


Figure 22: The covariance functions for the errors in the range and geophysical corrections sampled in 6 year mean Jason profiles.

Figure 22 shows the covariance functions associated with the approximate errors in the range and geophysical corrections in the South East Asian region. In this region the SSB errors clearly dominate the signal by a factor of nearly two and with very long correlation length of 220 km.

The wet troposphere correction is relatively large in this coastal region. However it is followed closely in magnitude by the ionospheric correction which is relatively large at low latitudes close to the Equator. The figure also shows that the correlation length of the wet troposphere correction is relatively short in this region whereas the correlation length for the other contributions is relatively long.

This difference in correlation length is also confirmed by the two dimensional covariance functions for each correction as shown in Figure 23 where it can be seen that the covariance function for the wet troposphere correction shows much more structure and shorter wavelength signals compared with the other corrections in the region.

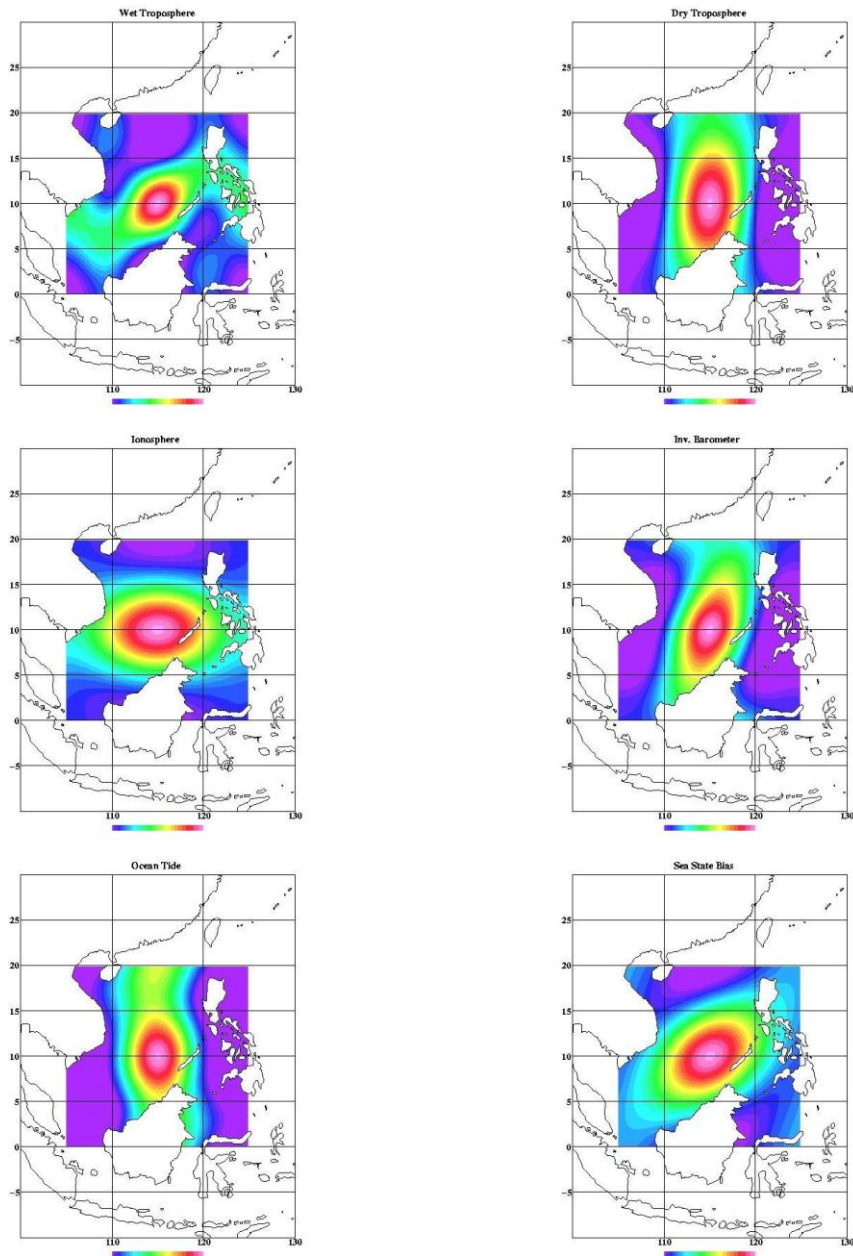


Figure 23: Two dimensional covariance function for the center of the North Atlantic region for each of the range and geophysical errors for 6 year mean Jason-1 profiles

3.2.4. Antarctic Region

The fourth and final region is region bounded by 60° S and 40° S, 40° W - 20° W in the southern Atlantic Ocean close to Antarctica and with the Antarctic Circumpolar Current passing through the region. The small South Georgian Islands can be seen in the plots but their presence does not affect the computation.

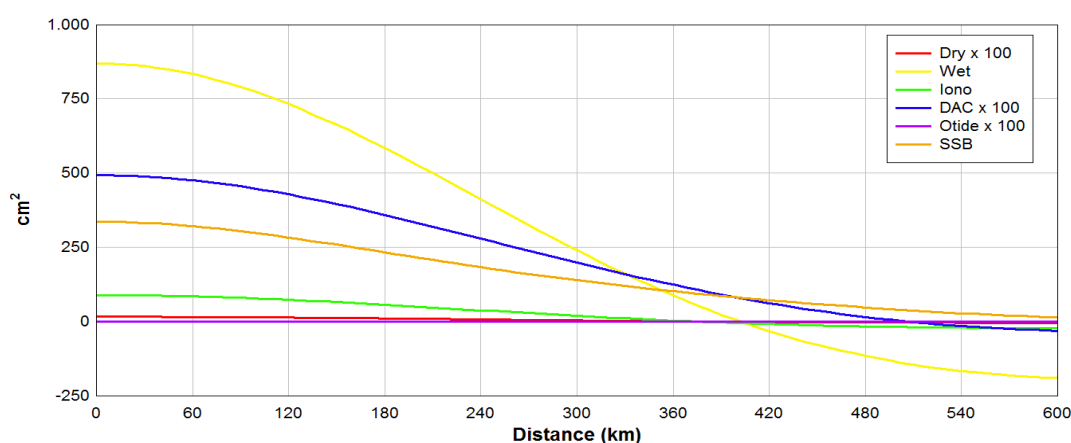


Figure 24: *The covariance functions for the errors in the range and geophysical corrections for 6 year mean Jason profiles. Notice that the scale on the vertical axis should be $10 \times \text{cm}^2$ like for the previous figures*

Figure 24 shows the covariance functions associated at high latitudes close to Antarctica. Even though the SSB is relatively large in this region, the wet troposphere corrections clearly dominate. Whereas the wet troposphere correction exhibited short wavelength in the previous coastal region in South East Asia it exhibit much longer correlation length at high latitude. Again the ionosphere, dry troposphere and ocean tide correction are nearly insignificant.

The final two dimensional covariance functions for each correction are shown in Figure 25. All these corrections exhibit longitudinal patterns at these latitudes which is very interesting and possibly related to the sampling by the satellite.

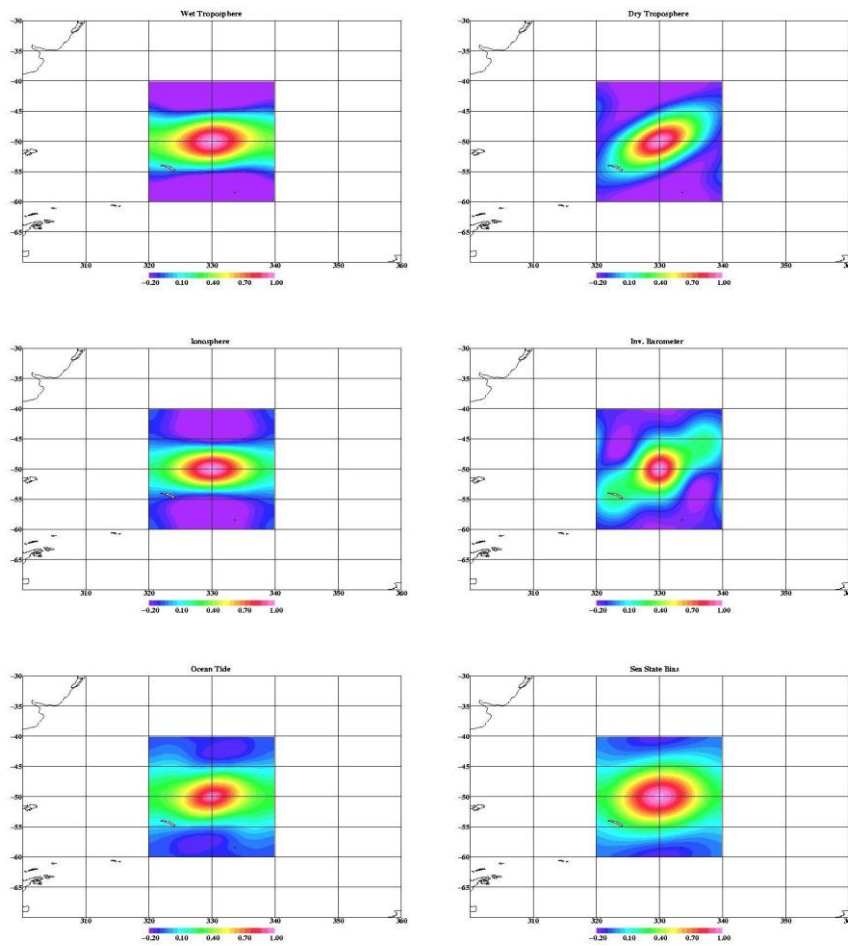
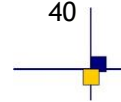


Figure 25: *Two dimensional covariance function for the Antarctica region for each of the range and geophysical errors for 6 year mean Jason-1 profiles*



4. MSS Error Approximation from Ocean State Estimation

In this study, we apply ocean state estimation using the 4DVar assimilation technique to approximate the error of the Mean Dynamic Topography (MDT), one of the constraints applied to the estimation process. Since the MDT applied is the filtered difference of a Mean Sea Surface (MSS) and a geoid, the error in the MSS can be obtained from the approximate MDT error and given a priori error information for the geoid.

Application of 4DVar for error estimation of its constraints needs several conditions to be fulfilled. In particular, realistic a priori errors for the constraints, the control variables as well as model errors have to be provided. Then, in a fully converged solution the expected model-data residuals are distributed in a χ^2 distribution around expectation values equal to the a priori errors given to the optimization. The comparison of model-data residuals with the a priori errors allows to test the reliability of the a priori errors.

We discuss here two optimization runs of the GECCO (German part of Estimating the Circulation and Climate of the Ocean) model. Both runs use the GOCO01s geoid model for calculating the MDT, but different MSS models are applied. In the first run we use CLS10, while in the second run, DTU10 is applied.

The comparison of the two runs allows to test the sensitivity of the model to different constraints for the MSS. A robust modelled MDT, not strongly depending on the chosen MSS model, would support a realistic representation of the MDT in the optimized solution. From the model-data residuals an estimate of the MSS error is deduced. It has, however, to be stated, that especially model errors and errors due to a not fully optimized solution will map into this estimate. Thus only a rough error estimate can be expected from this method. Since the MDT as a combined product composed from geoid and MSS is assimilated, rather than the MSS, the knowledge of the geoid error is required to deduce the MSS error from the error in the MDT. We take the a priori geoid error, which is provided with the geoid model, for this purpose.

4.1. Ocean Model and Data Assimilation Methodology

GECCO is based on the Massachusetts Institute of Technology general circulation model (MITgcm; *Marshall et al.* [1997]), which is a numerical implementation of the primitive equations formulated on z-levels on a spherical coordinate system.

The set-up we use for the optimizations here, is basically identical to the 50-yr run (1952-2001) of the GECCO model [*Köhl and Stammer*, 2008], also the initial ocean state is taken from this model synthesis. The syntheses use the adjoint method to bring the model into consistency with available hydrographic and satellite data as well as prior estimates of surface fluxes. The estimation of the control parameters was changed from a direct estimation of the fluxes every 10 days to the estimation of daily atmospheric state variables, which include surface air temperature, humidity, precipitation and the 10 m wind. The prior of the atmospheric state derives as in the previous estimate from the National Centers for Environmental Prediction (NCEP).

These control fields are then adjusted by the method to yield model states that are dynamically consistent with the model physics and the assimilated data within given error limits. We refer to Wunsch [1996] for a general introduction of the methodology. As before, the set of assimilated data includes altimeter data, AMSR/E SST, Argo temperature and salinity profiles.

The assimilation of MDT consists of a spatial MDT map as constraint of the modelled topography, and, since the geoid error is provided as spherical harmonic coefficients, the MDT cost function contribution is evaluated in spectral space.

The MSS model is transformed to SH coefficients, truncated at degree and order (d/o) of the geoid and transformed back to physical space. This methodology ensures, that the MSS is provided in the same spatial resolution as the geoid. The difference between MSS and geoid is computed and the resulting MDT is filtered using a Gaussian filter, with a filter scale just long enough to smooth out small scale noise.

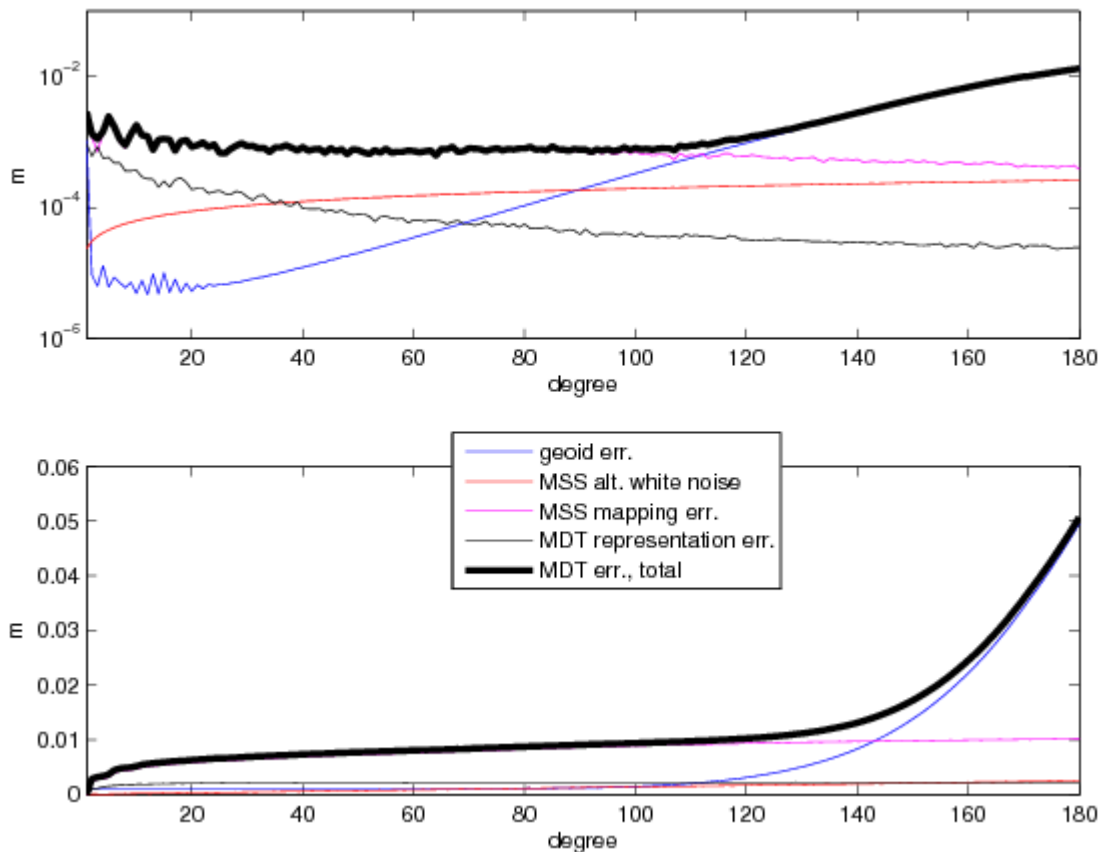
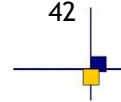


Figure 26: MDT error components given as square root of degree variances, for a given degree (top) and accumulated (bottom).



4.2. Ocean State Estimation Experiments

For the ocean state estimation experiments we targeted on reproducing the MDT together with other parameters of the ocean state as realistic as possible. The assimilation period is 7 years, from 1993 to 1999, identical to the reference period of one of the two MSS models (CLS2010) applied for calculating the MDT. The second MSS model applied (DTU10) is valid for 1993-2009 and is thus re-referenced using Sea Level Anomaly data. The geoid applied is the first available combined GRACE-GOCE solution (GOCO01s). To obtain spectrally consistent MSS and geoid maps, both MSS maps are spectrally filtered by cutting-off all signals beyond d/o 224, the resolution of the GOCO01s model. After subtracting the geoid from the filtered MSS, a spatial smoothing with a 1.2° Gaussian filter is performed to smooth out small scale noise.

The MDT error estimate is displayed in Figure 26. It consists of the error in the geoid, provided with the geoid, the error in altimetry (4 cm white noise for each single observation), the representation error of the hydrodynamic model due to limited spatial resolution (estimated as one half of the R.M.S. signal in Sea Level Anomaly from satellite altimetry), and the mapping error of the MSS. Since high resolution geoid information is taken into account when estimating the MSS (see [\[products/auxiliary-products/mss/mss-description/index.html\]\(http://www.aviso.oceanobs.com/en/data/products/auxiliary-products/mss/mss-description/index.html\) for more information\), we estimate only the mapping error of the MDT. To do so, we simulate altimeter observations by sub-sampling a high resolution modelled MDT \(from the POP model, see *Maltrud and McClean, 2005*\) along the ground tracks of the JASON and EnviSat altimeters. By interpolating the 'observed' data to the GECCO model grid and comparing it with the original MDT, we get an error estimate for the MDT mapping, that is then projected to spherical harmonic functions.](http://www.aviso.oceanobs.com/en/data/</p></div><div data-bbox=)

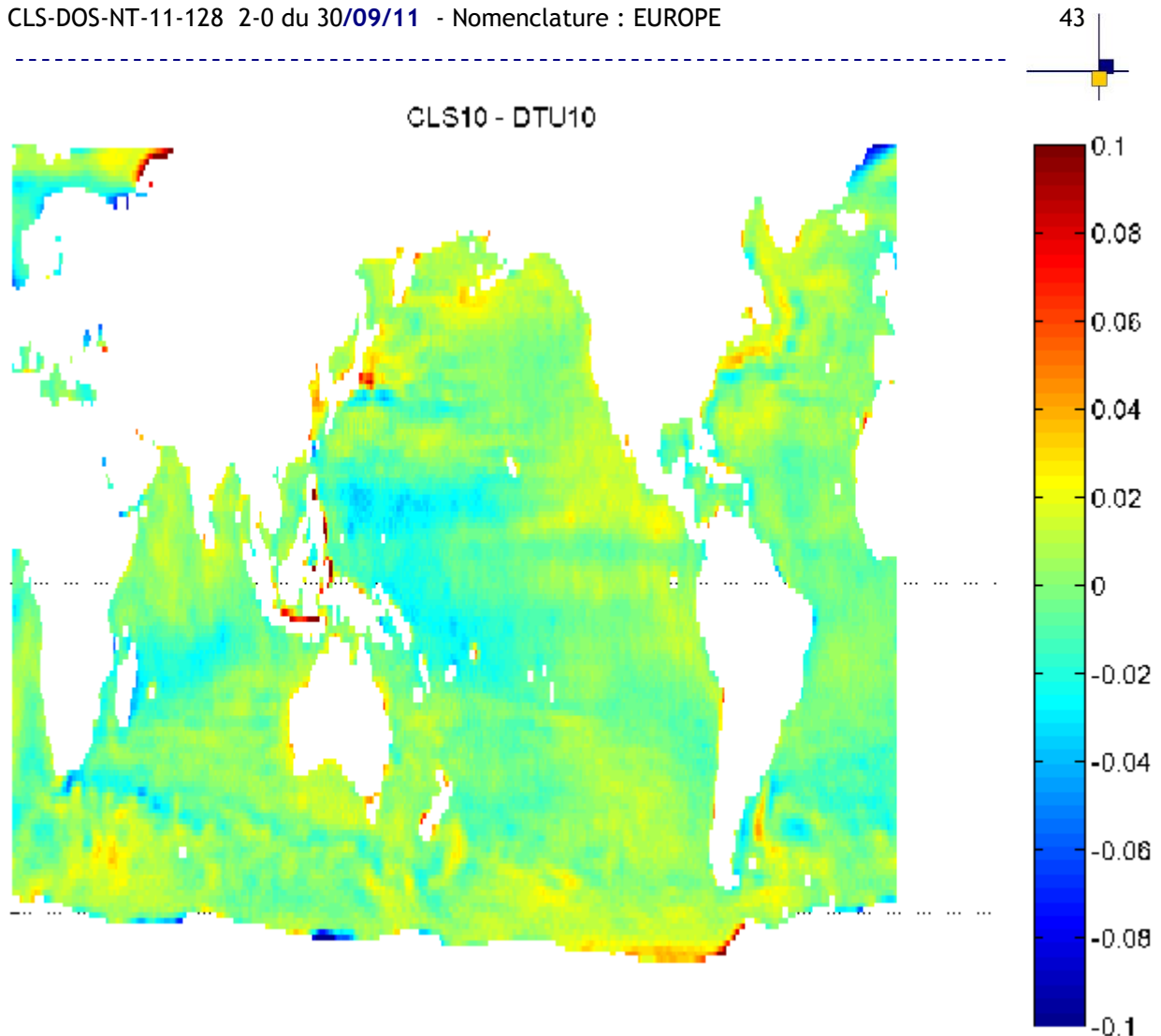


Figure 27: Difference in assimilated MDT [m], depending on the applied MSS (CLS10-DTU10).

Two optimizations are performed. The only difference between these integrations is the MSS applied for calculating the MDT, while otherwise the set-up is identical, including the a-priori error information. The two optimizations are referred to as GECCO-CLS and GECCO-DTU, depending on the MSS model used.

4.3. MSS error approximation

Figure 27 displays the difference between the two MDTs, that is, the filtered difference of the two MSS models (CLS10-DTU10).

Strong differences are found along the coastlines in (partly) ice-covered polar regions and in Indonesia, and also along the Gulf Stream and the Kuroshio. Otherwise the misfits are dominated by large scale, basin wide, signals, with amplitudes hardly exceeding 3 cm. The overall R.M.S. difference of the two MSS models is 1.6 cm.

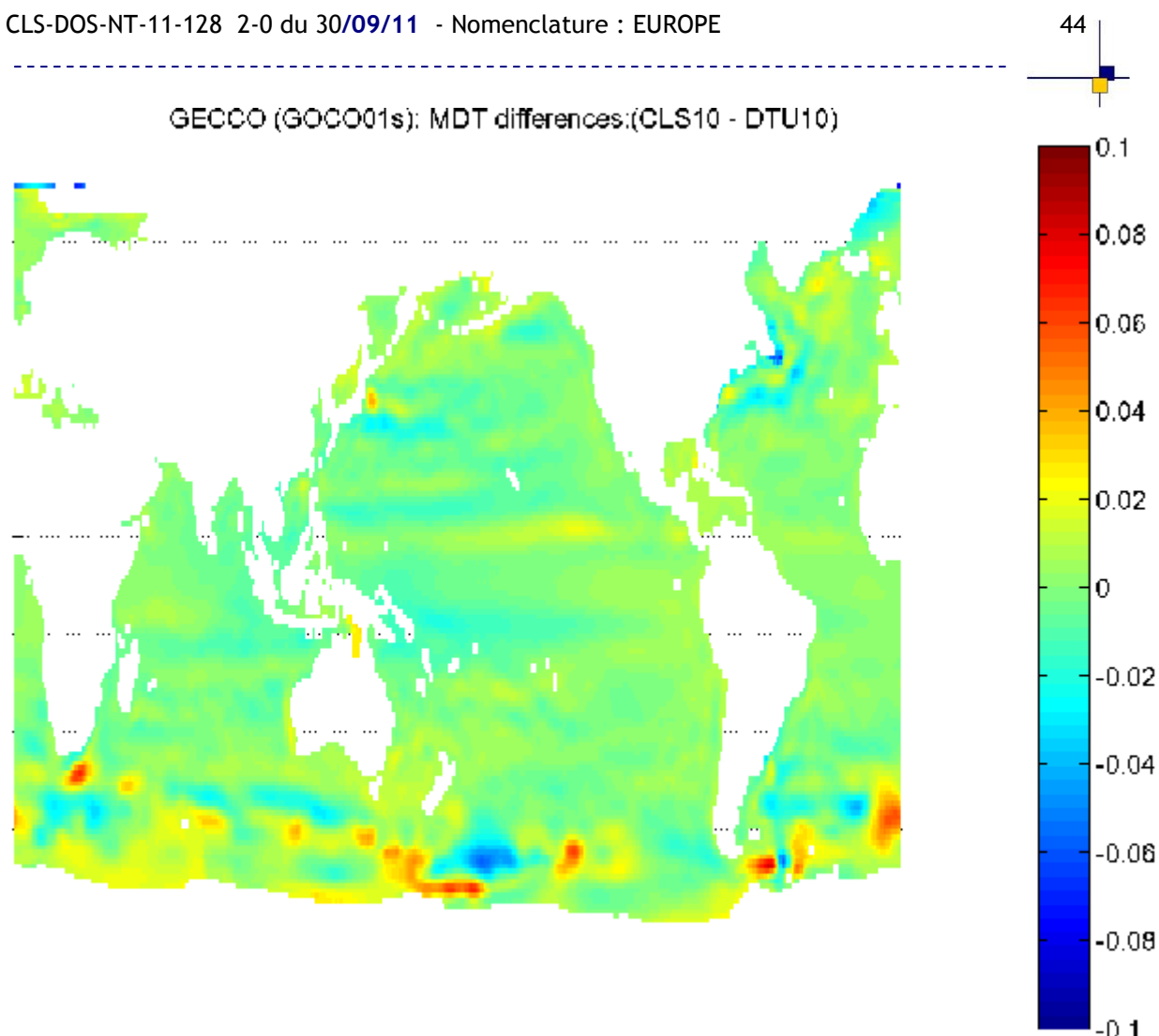


Figure 28: Difference in modeled MDT [m] (GECCO-CLS - GECCO-DTU)..

Figure 28 displays the difference in optimized MDT from the two model integrations.

Both solutions are (almost) converged, after 69 (CLS10) and 89 (DTU10) iterations. Apart from some stronger differences in the order of 5 cm in the Antarctic Circumpolar Current (ACC) the differences are generally smaller than the differences in the MSS, meaning that the modelled MDT is a rather robust signal, not strongly depending on the MSS assimilated. This is an interesting result since assimilation of an MDT, in addition to other, usually assimilated data sets, strongly impacts the modelled MDT (also not shown, but see Siegismund et al., 2011).

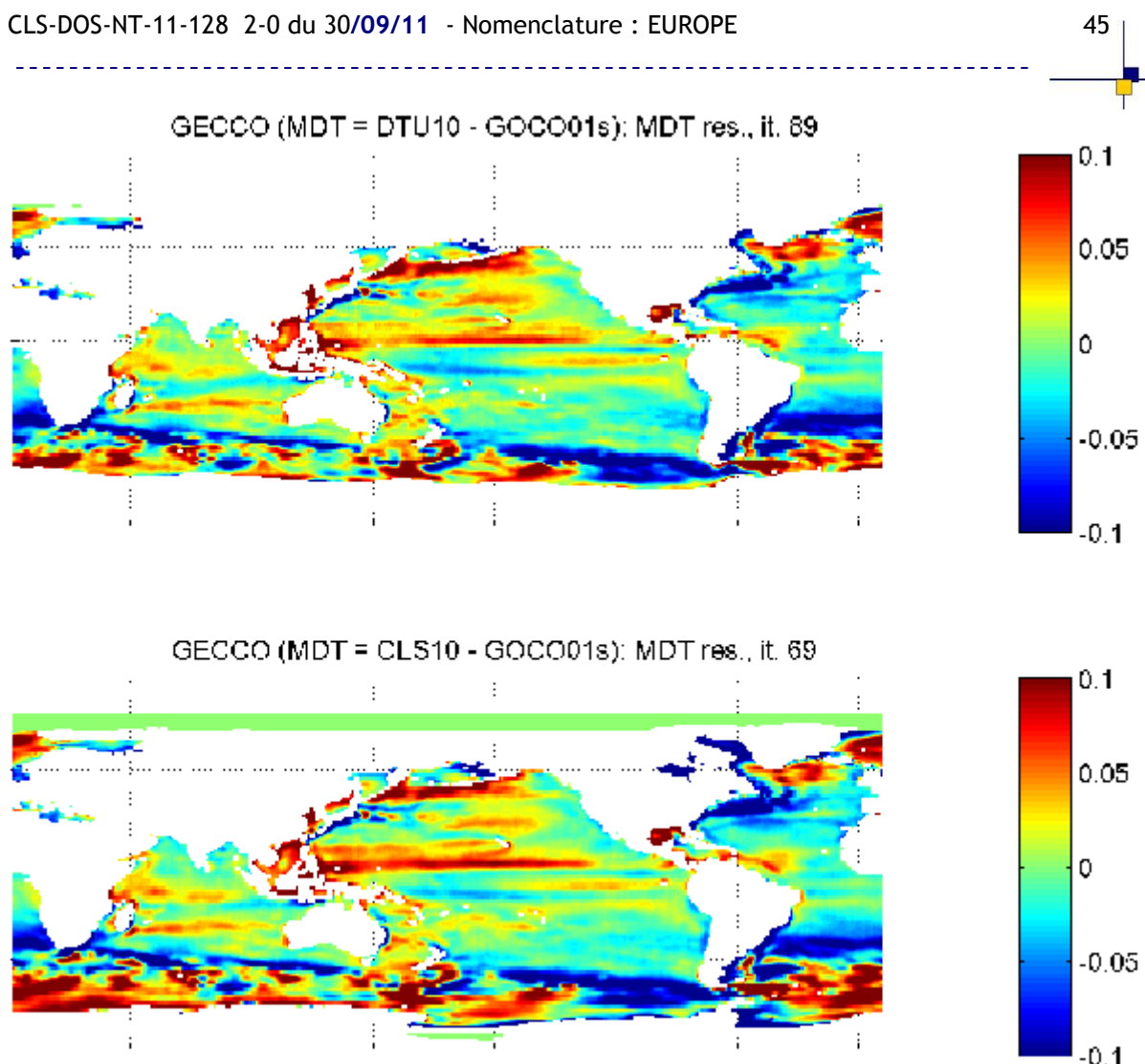


Figure 29: MDT residuals [m] for converged GECCO solutions for (top) GECCO-DTU and (bottom) GECCO-CLS.

The MDT residuals are displayed in Figure 29. Clearly, the residuals are generally larger than the difference of the MSS models assimilated (see Figure 27), with strongest signals in the Southern Ocean. The spectral representation (Figure 30, for GECCO-CLS) reveals the residuals being higher than the a priori errors up to approximately degree 130. However, the filtering of the MDT with the 1.2° Gaussian kernel is not taken into account for the a priori errors and might be strongly overestimated for the high degrees.

Ignoring the error in the short scales beyond degree and order 120 gives an a priori error of approximately 1 cm, predominated by the mapping error of the MSS (see Figure 26), while all other error components can be disregarded to first order.

It has to be stated, that the true error in MSS might contain considerable signal also on the long scales from range and POD errors other than the 4 cm white noise we consider here. The poor knowledge of those errors prevented to use them here.

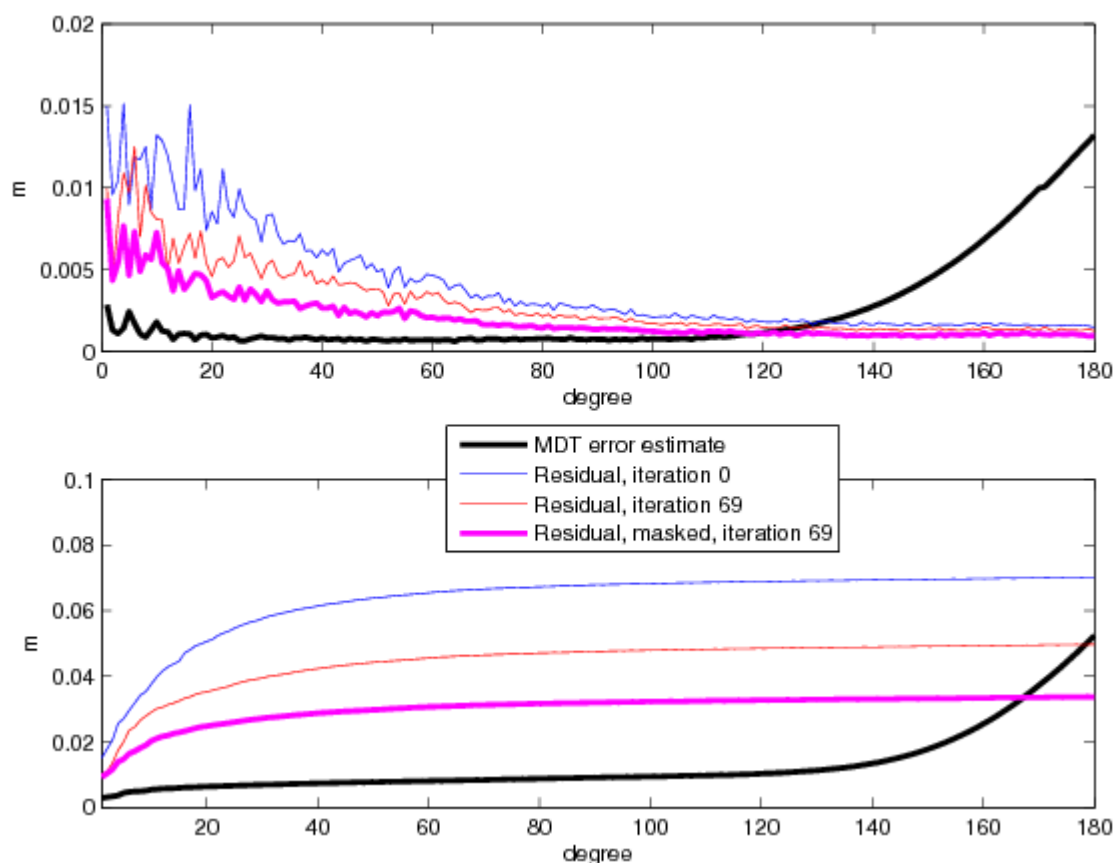


Figure 30: MDT residuals [m] from GECCO-CLS optimization compared to a priori MDT error, given as square root of degree variances for specific degree (top) and accumulated (bottom).

From the comparison, to correct for the inconsistency between residuals and a priori error, for both integrations, an increase of the MSS error from 1 cm to 6 cm, overall, would be necessary.

However, for part of the global ocean, especially for the ACC and the western intensified currents, as the Gulf Stream and the Kuroshio, the associated mesoscale variability and its influence onto the mean circulation has to be parameterized in the model and leads to model errors in those regions, that are not taken into account in the present optimizations and will thus map into the MSS error estimations.

Masking out the ACC, the Gulf Stream and the Kuroshio and taking only into account discrepancies of residuals and a priori error in the remaining part of the ocean reduces the overall MSS error estimate to 4 cm (see Figure 31 for GECCO-CLS). One has, however, to keep in mind, that the MSS might contain considerable errors in the regions masked out due to unresolved (or aliased) small scale signals, which are not taken into account in this error estimate.

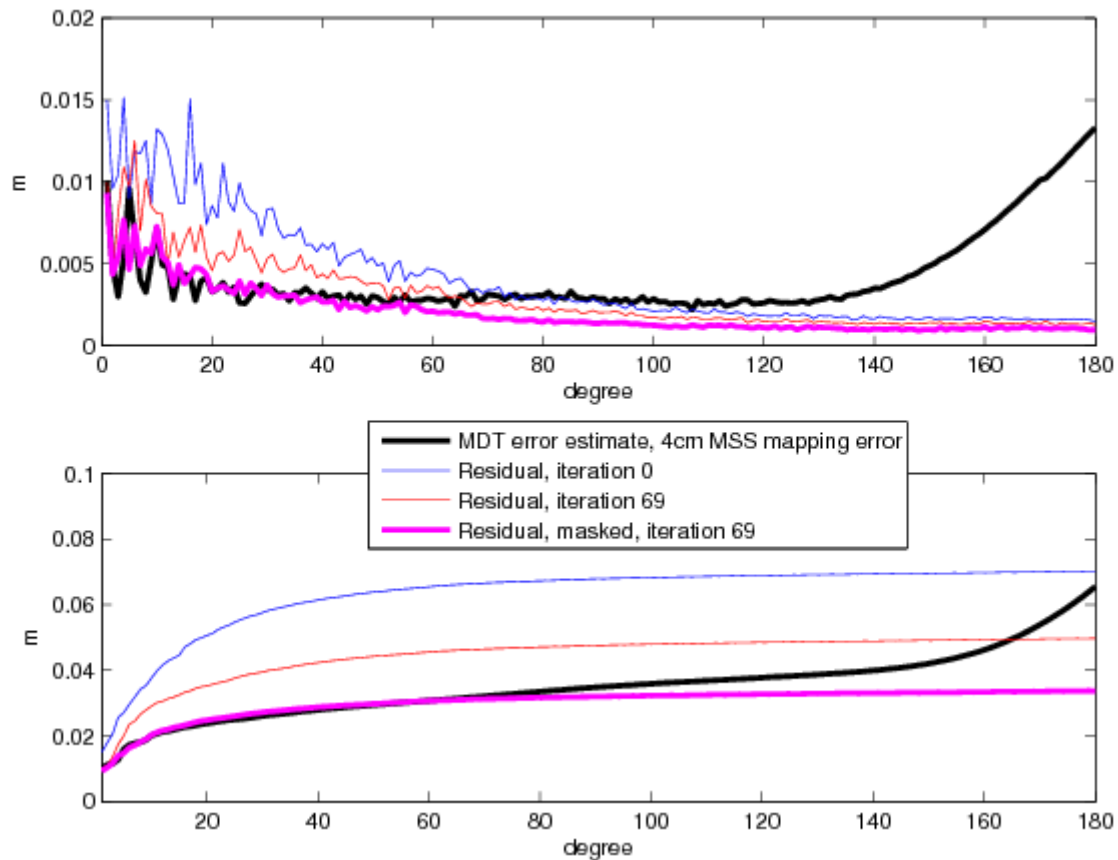


Figure 31: Same as Fig. 30, but with increased MSS mapping error.

However, given the robust MDT signal of the model, and the fact, that both, MDT errors due to a not fully converged model solution and model errors are included in our MSS error estimate, the 4 cm overall error is an upper estimate of the MSS, at least, if regions of strong mesoscale activity are disregarded.

This error estimate is larger than the R.M.S. difference of the two models (1.6 cm). Beside the mentioned possible overestimation this might also point to errors common in both MSS models and thus not seen in the R.M.S.

Annexe A - List of acronyms

TBC	To be confirmed
TBD	To be defined
AD	Applicable Document
RD	Reference Document